Searching for Life on Titan:
The Undersea Retrieval of Titan Lake Extractions (TURTLE) Mission

Maximilian Adang [*], Arielle Ainabe [†], Aditya Dave [‡], Adrian Dumitrescu [§], Anna E. Engle [¶], Sarah Lamm [‖], Connie Liou [**], Samuel Y. W. Low [††], Corey McClelland [‡‡], Giuliana Miceli [§§], Palak Patel [¶¶], Pedro Salazar [***], Leanne Su [†††], Jessica Todd [‡‡‡], Adam Vigneron [§§§], Brit Wylie [¶¶¶]

The Undersea Retrieval of Titan Lake Extractions (TURTLE) is a proposed mission concept and full system design for a Titan lander with sample collection and return as its primary objective. Uniquely, Titan is the only other known body in the solar system, aside from Earth, to host stable bodies of liquid on its surface. Additionally, the Saturnian satellite is shrouded in a thick nitrogen-rich atmosphere that supports ongoing atmospheric methane photochemistry, creating an array of complex hydrocarbons and nitriles. And, given its surface temperature range of 89-95 K, the surficial liquids are not water, but rather a mixture of methane, ethane, and dissolved nitrogen. These attributes make Titan a target of interest, both for its familiar yet exotic surface processes and for its astrobiological potential. The TURTLE mission aims to further our understanding of Titan through observing atmospheric tholins, analyzing lake Ligeia Mare at various depths, and characterizing the solid organic lake sediments. The proposed TURTLE lander is equipped with three instrument suites: *Sirens* (a gas chromatograph and laser desorption mass spectrometer), *BlastCam* (a Raman and laser-induced breakdown spectroscopy with underwater capabilities), and *TitanCam-Z* (a multispectral spectrographic imager). In addition to the missions' remote and in situ measurements, we propose to return samples of the atmosphere, lake liquids at various depths, and lakebed sediments. The Titan TURTLE mission concept proposes the first sample return mission from Titan, as well as the first liquid return samples from any other celestial body.

[*]Maximilian Adang is an undergraduate student at Caltech, Dept. of Engineering and Applied Sciences madang@caltech.edu
[†]Arielle Ainabe is an undergraduate student at McMaster University, Dept. of Engineering Physics ainabea@mcmaster.ca
[‡]Aditya Dave is a PhD candidate at the University of Minnesota, Dept. of Electrical and Computer Engineering, davex033@umn.edu
[§]Adrian Dumitrescu is a PhD candidate at University of Southampton, Dept. of Aeronautics and Astronautics, a.dumitrescu@soton.ac.uk
[¶]Anna Engle is a PhD candidate at Northern Arizona University, Dept. of Astronomy and Planetary Science aee98@nau.edu
[‖]Sarah Lamm is a PhD student at The University of Kansas, Dept. of Geology slamm@ku.edu
[**]Connie Liou is a PhD candidate at Stanford University, Dept. of Aeronautics and Astronautics connie.liou@stanford.edu
[††]Samuel Low is a MSc student at Stanford University, Dept. of Aeronautics and Astronautics sammmlow@stanford.edu
[‡‡]Corey McClelland is a graduate student at the School of Visual Arts, New York City cmcclelland1@sva.edu
[§§]Giuliana Miceli is a PhD candidate at CU Boulder, Colorado Center for Astrodynamics Research giuliana.miceli@colorado.edu
[¶¶]Palak Patel is a PhD Candidate at Massachusetts Institute of Technology, Dept. of Mechanical Engineering palak@mit.edu
[***]Pedro Salazar is an undergraduate student at Iowa State University, Dept. of Industrial Engineering pjose@iastate.edu
[†††]Leanne Su is a PhD candidate at the University of Michigan, Ann Arbor, Dept. of Aerospace Engineering leannesu@umich.edu
[‡‡‡]Jessica Todd is a PhD candidate at Massachusetts Institute of Technology, Dept. of Aeronautics and Astronautics, jetodd@mit.edu
[§§§]Adam Vigneron is a doctoral candidate at Airbus Defence and Space, Science Future Programs Department, adam@vigneron.ca
[¶¶¶]Brit Wylie is an undergraduate student at Caltech, Dept. of Engineering and Applied Sciences wybrit98@gmail.com

Authors are listed alphabetically.

I. Introduction

The Undersea Retrieval of Titan Lake Extractions (TURTLE) is a proposed Titan sample return mission, with an aimed launch date on 24 October 2038, an entry date into the Saturnian system on 12 September 2046, a rough mission window of 1 year and a proposed departure date in July 2049, contingent on successful sample collection.

The broad science goal is to determine Titan's habitability and potential for extant and/or extinct life. TURTLE will utilize the moon's second largest lake, Ligeia Mare, as a means of assessing the presence of biologically relevant molecules and features typically associated with biological processes. The mission objectives are to capture three sample states of Ligeia Mare: 1) the lake liquid, 2) the atmosphere layer directly above the lake surface, and 3) the lakebed sediments. Additionally, during the descent, TURTLE will perform in-situ measurements of atmospheric tholins. Prior to the ascent phase, the mission will execute in-situ measurements on all fluid and solid samples to analyze their chemical composition, mineralogy, and the carbon isotope ratio. Data will be communicated back to Earth in case the ascent stage (sample return) fails.

The engineering goals are to design a system comprised of an orbiter and a lander. The orbiter functions as a transport vehicle for the lander and samples from Earth to Saturn and back. It also serves as a topographical survey vehicle during early operations prior to descent. The lander is a buoy with an ascent vehicle housed within and will carry all sample collection and measurement instrumentation. The mission will comply with planetary protection guidelines to avoid surface contamination of Titan with elements from Earth, so as to preserve a pristine environment and prevent false detection of organic compounds erroneously carried from Earth. The extreme low temperatures of Titan poses a challenge to preserving the physical, chemical, mineralogical, and thermal integrity of the samples throughout the mission. Thus, cryogenics are also a critical design factor in our proposal.

This mission proposal was conceived from scratch during the Caltech Space Challenge 2022—a highly competitive, week-long, international space mission design competition under the mentorship of experts from industry, academia, and NASA Jet Propulsion Laboratory. This mission is novel in its focus on returning samples in the solid, liquid and gas phases simultaneously.

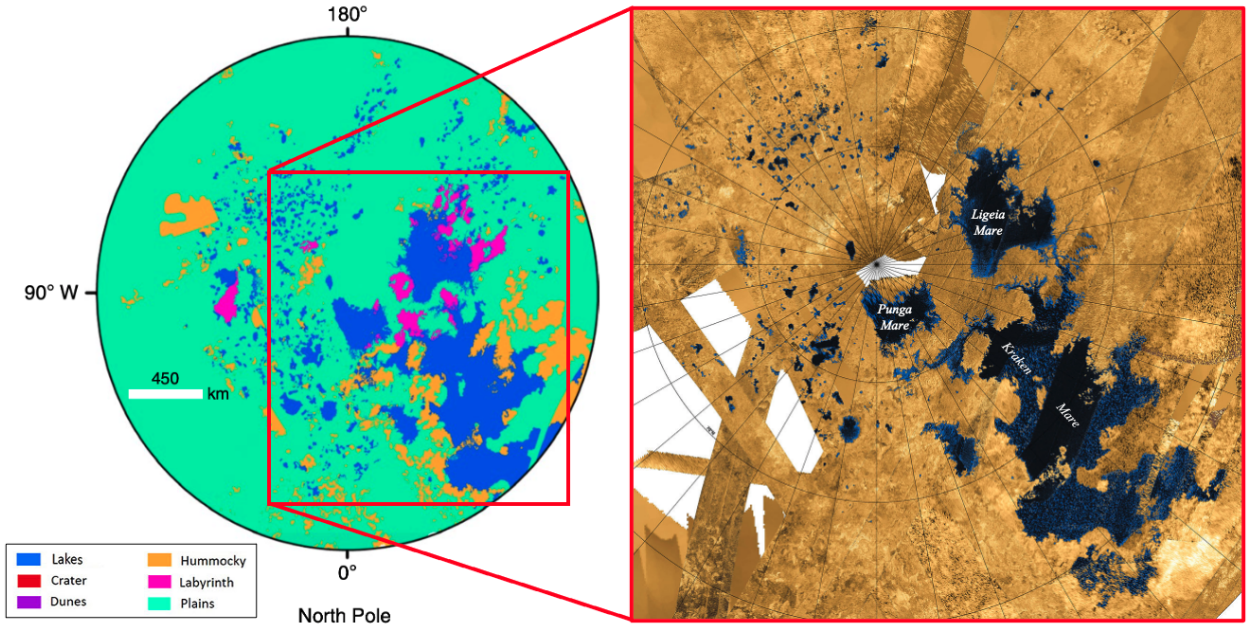

Fig. 1 ***Left:*** **A 1:20,000,000 scale map of the major geological units of Titan's north polar region [1].** ***Right:*** **A Synthetic Aperture Radar (SAR) mosaic of Kraken, Ligeia, and Punga Mare, the three largest bodies of liquid on Titan's surface. Ligeia Mare is the intended landing site of TURTLE (Credits: NASA/JPL/Caltech/ASI/USGS).**

II. Mission Justification

Titan, Saturn's largest moon, is unique among the solar system satellites in its diverse range of surface and atmospheric processes that are akin to what we find on Earth. It has the most substantial atmosphere of any satellite in our solar system and is composed predominately of nitrogen [2–4]. Its surface contains geological features like dunes and mountains [1], as well as stable bodies of liquid [1, 5]. As with Earth, these components interact with one another in complex processes, albeit with quite different materials.

With surface temperatures ranging between 89-95 K and a surface pressure of ~1.5 bar [6], water is frozen on Titan and methane takes its place, creating a methanolgical (as opposed to hydrological) cycle. Methane rains down [7, 8] and the precipitation forms lakes in the north and south polar regions. Ethane is the second major constituent of the liquid composition and is the most common hydrocarbon by-product of the atmospheric methane photochemical process [9]. Like methane, ethane settles into the lakes either by falling directly in or by being deposited through fluvial processes. The third, and last, bulk molecular species in the lakes is dissolved atmospheric nitrogen. Together, the three primary species add a layer of complexity to the lacustrine environment due to their non-ideal behavior [10–12].

The lakes are almost exclusively located at Titan's poles [5]. Currently, most of the surface liquid is found in the north polar region, as the area tends to experience longer, cooler summers in comparison to the south. It is this region that is home to the three largest lakes, which are Kraken Mare (5.0×10^5 km^2), Ligeia Mare (1.3×10^5 km^2), and Punga Mare (6.1×10^4 km^2) [13] (Fig. 1), with all three likely having depths between 100-300 m [14]. The presence of the polar lakes gives rise to the question of potential habitability and the existence of life, particularly in the form of life as we *do not* know it. McKay & Smith (2005) [15] assert the possibility of methanogenic life by providing a possible energy source created by the interactions of acetylene (C_2H_2), ethane (C_2H_6), and organic haze (R-CH_2) with atmospheric hydrogen (H_2). By calculating the Gibbs free energies of all three reactions, we find -ΔG = 334, 57, and 54 kJ/mol for C_2H_2+H_2, C_2H_6+H_2, and R-CH_2+H_2 respectively. This compares favorably to the 42 kJ/mol minimum energy required to power methanogen growth on Earth [15]. The apparent depletion of tropospheric molecular hydrogen plus the existence of surface acetylene deposits further inspire the possibility of hydrocarbon-based life [13]. There are a number of other driving factors that indicate the potential for extant or extinct life on Titan, such as a surplus of methane in the atmosphere and a reported carbon ratio ($^{12}C/^{13}C = 95 \pm 1$) that is consistent with a biological origin [16].

Of course, there are arguments refuting Titan's lake habitability that should be considered, such as the low temperatures that result in low reaction rates and the low organic solubility into liquid methane [15]. Even if no life is found, a lake-based mission could address other outstanding questions, like the mysterious replenishment source of methane, the location of the missing ethane, an explanation for the higher light carbon ratio, the potential for the lakes to be part of karst systems, and many more.

The recently selected Dragonfly mission is a rotorcraft lander that will explore the equatorial region, namely in the context of searching for prebiotic materials, and is scheduled to arrive at Titan in 2034 [17, 18]. While this is an exciting time for the Titan community, it is not anticipated that Dragonfly will make it to the poles to explore the lakes. The mission proposed in this paper is for a lake sample return mission that would be the first of its kind; a buoy-and-probe lander that is designed to collect and return samples from Ligeia Mare in the form of all three common states—gas, solid, and liquid. The return samples will include material from: (1) the atmosphere directly above the lake surface, (2) the lake liquid itself, and (3) the solid sediments in the lake beds. The primary objectives will be looking for both biotic and prebiotic signatures in the atmosphere, lakes, and lake beds, along with assessing the habitability of Titan's lakes. Additionally, performing measurements *in situ* and returning samples to Earth can help address fundamental questions behind some of the themes set forth by the National Research Council (NRC) in the 2023-2032 Decadal Survey [19].

III. Science Objectives and Instruments

The principal driver behind this mission proposal is to assess the potential for life and habitability using Titan as a planetary laboratory. Building upon insights gleaned from Cassini-Huygens' success [20] and complementing the scientific objectives of the future Dragonfly mission launching in 2027 [17, 18], two primary scientific objectives are derived from the broader science goals set by the NRC Decadal Surveys. The first is to determine if biologically relevant chemical components are present in the atmosphere, liquid, and/or seafloor of Ligeia Mare. The second is to assess whether the features representative of biological processes exist in the atmosphere, liquid, or lake bed of Ligeia Mare.

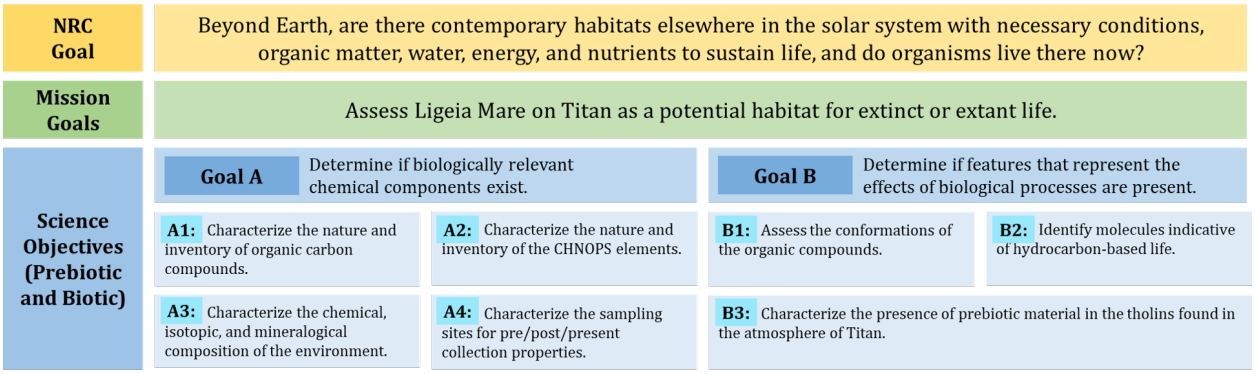

Fig. 2 Science Traceability Matrix (STM): charting the NRC goal to specific science objectives.

From these two primary objectives, specific sub-objectives are laid out in support of the broader goals in our science traceability matrix (STM) as shown in Fig. 2. The prerequisite measurements, and thus the supporting instruments with desired functional specifications, can be determined in a dependency flow as per Fig. 3. Thus, the STM drives the selection of the landing probe's instruments in Fig. 4.

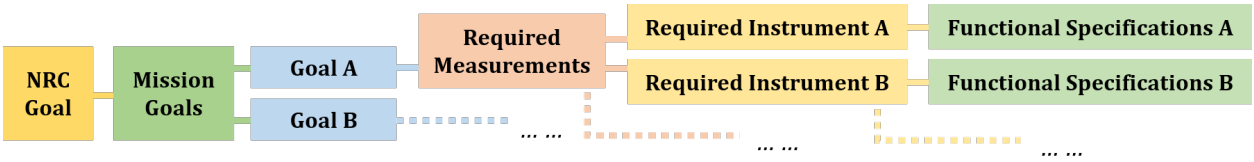

Fig. 3 STM dependency flow of measurement requirements and instrument specs from science goals.

The instruments in Fig. 4 were selected to answer all science objectives as they can assess the chemical composition, molecular structure, and isotopic characteristics on solid, liquid, and gases with a special focus on organic materials. They also have flight heritage: *Sirens*' predecessor was used in Huygens' landing on Titan and a similar model will be part of the Dragonfly rotorcraft, while *BlastCam* and *TitanCam-Z* are derived from Curiosity and Perseverance.

Determine if biologically relevant chemical components exist. ← **Goals** → **Determine if features indicating effects of biological processes are present.**

Name	Instruments	Measurements	Predecessors
Sirens	Gas Chromatograph and Laser Desorption Mass Spectrometer	Chemical composition, molecular structure, and chirality of the atmosphere on descent and directly above lake surface	Successor of the GC-MS on Huygens, DraMS on Dragonfly, from SAM (Curiosity), and MOMA (ExoMars)
BlastCam	LIBS, Raman, and Passive Spectroscopy	Chemical composition, molecular structure, chirality, and mineralogy of the lake liquid and seafloor	Derived from, ChemCam (Curiosity), SuperCam, InVADER, and SHERLOC (Perseverance). Uses lessons from RLS (ExoMars) and MarSCoDe (Zhurong)
TitanCam-Z	Multi-spectral, Spectrographic Imager	Morphology, structure, and texture of atmospheric tholins; provide environmental context of lander position	Direct successor of Mastcam-Z (Perseverance) and Mastcam (Curiosity)

Fig. 4 Proposed three instrument suites on the lander. ***Predecessors:*** **Sirens: [17, 18, 21–24]; BlastCam: [25–32]; TitanCam-Z: [33–35]**

IV. Mission Overview

A. Overview of Mission Concept

The mission assumes the commercial availability of a SpaceX Starship-like launcher by the intended launch date in October 2038. The choice of launch vehicle is derived from overall system sizing (size, weight and power) of the landing buoy and the orbiter (see Section IV.C). its buoyancy requirements and the orbiter sizing, The overall mission concept relies on a single launch with SpaceX's Starship in October 2038 with the expected arrival year at Titan in approximately 2048. Starship will launch the Titan Orbiter with the landing vehicle attached. The orbiter-lander will use a single NASA Evolutionary Xenon Thruster (NEXT) for the ten year interplanetary journey [36], and a chemical propulsion system for high-thrust orbit insertion. Once the orbiter-lander is in Titan's orbit, a pre-landing characterization of Titan will be made. The orbiter will feature two instruments with Cassini heritage which will help with the landing: a surface imager based on VIMS and a wind profiler based on CIRS [37]. The imager will map Ligeia Mare and support the descent trajectory, while the wind profiler will characterize the upper atmospheric winds on Titan to restrict the size of the landing ellipse for the Lander. After the pre-landing characterization, the lander will descend onto Ligeia Mare while the orbiter will stay in a circular orbit inclined at 78° at 1550 km altitude around Titan. The surface operations will commence with an expected duration of 50 days. Once the surface operations have been completed and the atmosphere, liquid, and gas samples have been collected, the ascent vehicle will deliver the sample container into Titan's orbit where it will be retrieved by the orbiter. The orbiter will then depart from the Saturnian system in September 2050, with an Earth final arrival date of January 2059, for an approximate total mission duration of 20 years and 3 months. See Fig. 5 for a visual summary of the high level concept of operations of the TURTLE mission.

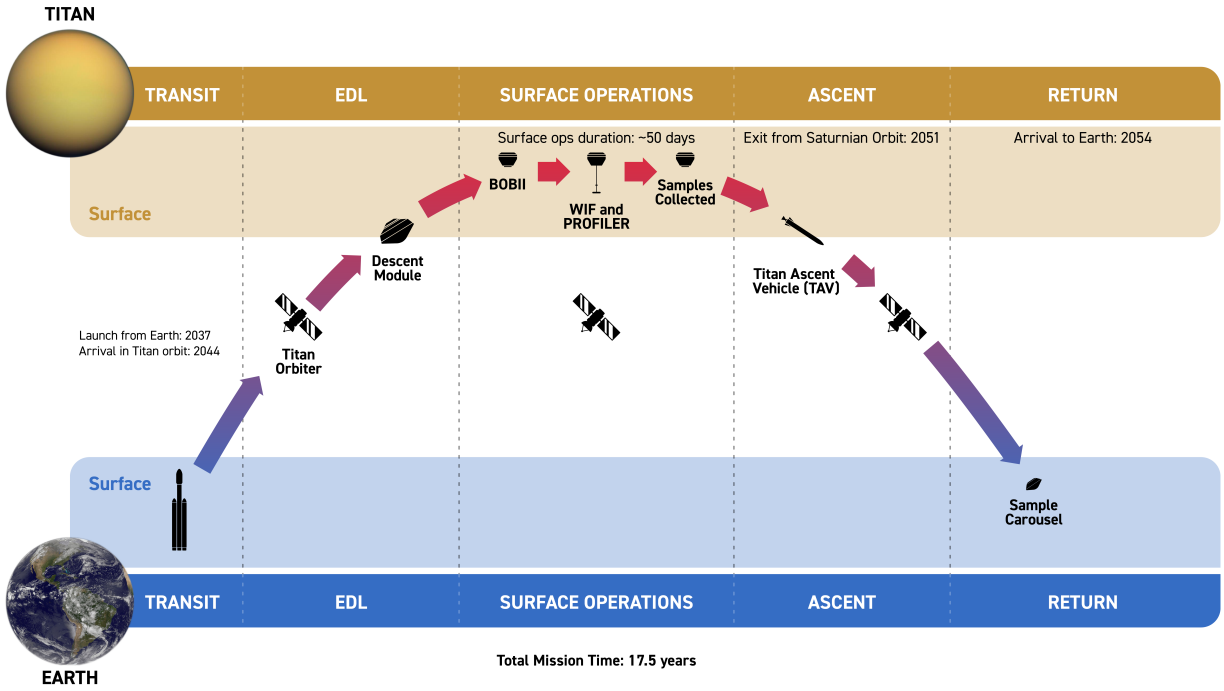

Fig. 5 Overall mission concept of operations (CONOPS).

To arrive at the final mission concept a set of trade-off studies was performed, with the most important revolving around the landing system. This is because the lander is the key to the entire mission: it will collect all of the samples and it will be responsible for launching them safely from Titan's surface. Four main concepts were considered: rovers, watercraft, rotorcraft, and a buoy system with a profiler. They are depicted in Fig. 6.

The first option focuses on a rover which would land on a flat surface near Ligeia Mare. The rover would collect the soil sample from the shoreline as it would not have access to the lake floor. Both the atmosphere and the lake sample

would be collected by attaching the relevant instruments to an extendable arm that would protrude just above the lake surface. The downside in terms of sample collection is that doing a vertical profile of the lake is not possible, while the horizontal profiling will also be limited by the length of the extendable arm. The descent would also be an issue because the landing accuracy required is around 25 to 50 km in order to avoid both the lake and the cliffs with the terrain still not being perfectly flat, while the Dragonfly landing ellipse is 149 km by 72 km due to the low resolution imaging of Titan's surface. On the other hand, the ascent from the surface of Titan is straightforward because it is land based and it has legacy from the Apollo missions.

The second option involves a splashdown into Ligeia Mare which is simple by comparison because of the low landing accuracy required. The boat would have a profiler attached on the underside to be able to produce a vertical profile of the lake liquid. The boat would have the capability of moving across the lake surface to also provide a horizontal profile, while collecting the atmosphere sample without much difficulty. The soil sample would be collected from the lake floor via the profiler. The main issue with the powered boat - profiler system is the complexity and the number of dynamic components. The ascent from Titan is also difficult because the launch will occur from the lake, rather than from the land. Moreover, the system mass and power can be an issue.

The third option is very similar to the previous concept, but it removes the horizontal movement on the lake surface. As a result, the boat is replaced by a floating buoy which has the profiler integrated in its lower half. The sample collection remains the same, but there is no horizontal profile available for the lake liquid. However, the system complexity and power requirements are decreased by having a static buoy.

Finally, the fourth option is similar to the Dragonfly mission and it involves a multi-rotor vehicle. The vehicle will be able to collect solid samples from the lake shore, while flying above the lake to collect the atmosphere and lake samples. Collecting the lake and atmosphere samples can be problematic because of the disturbance caused by the rotors.

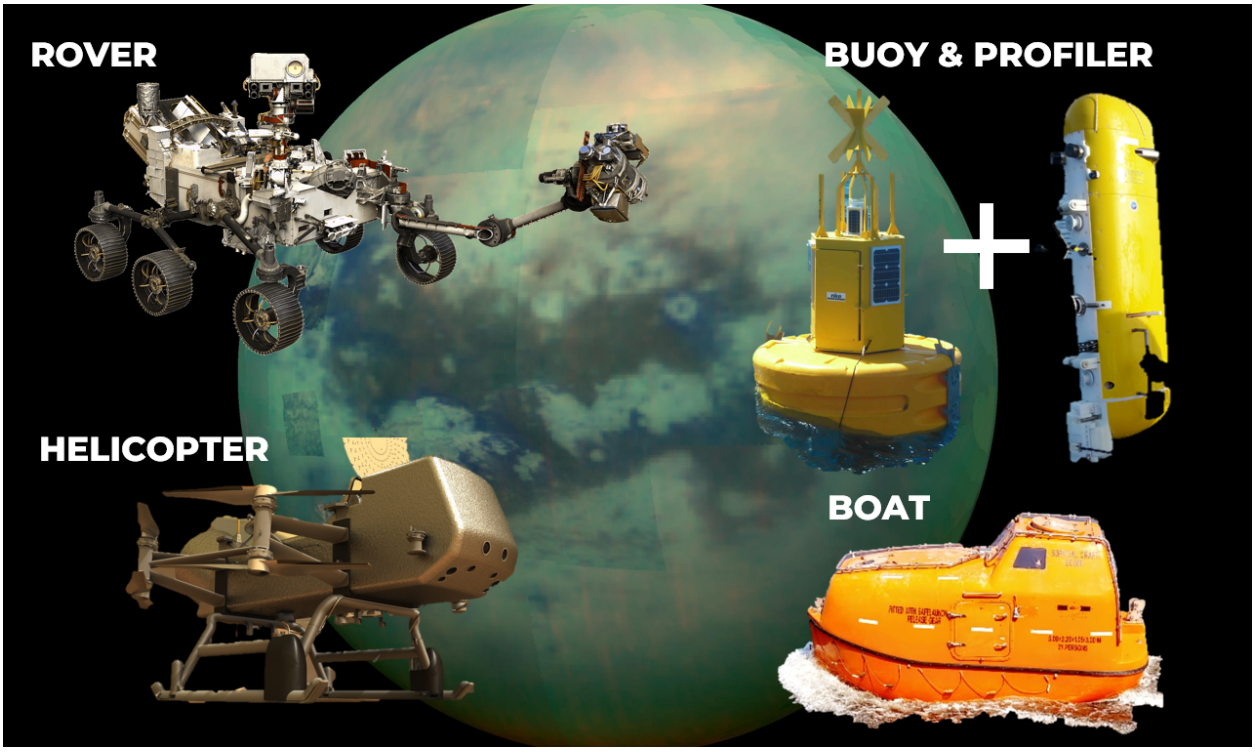

Fig. 6 The four lander options: rover, rotorcraft, buoy + profiler and the moving boat

Considering the importance of the vertical lake profile together with the similarity of the rover and multi-rotor solutions to previous missions (Perseverance and Dragonfly respectively), the boat and the buoy options are the most viable. Choosing between the two, the complexity of the moving boat means that the buoy system should be more reliable.

The overall mission concept features three total vehicles: one orbiter, one lander and one ascent vehicle. The lander will

splashdown onto Ligeia Mare because landing on the surface next to the lake would require a very small landing ellipse and landing on the lake allows the collection of a richer variety of samples. The lander itself is depicted in Fig. 7 and it features a buoy which floats on the surface of the lake and a profiler which can provide a vertical profile of the lake liquid. The buoy will hold all the subsystems critical to the operation of the lander, including the ascent vehicle and the Sirens instrument which will collect the atmospheric samples. The profiler will feature fiber optics cables which will run to the BlastCam and the TitanCam-Z which are sat in the buoy and it will collect liquid samples, while the Weighted Instrument Frame (WIF) will fix the buoy to the lake bed to collect the solid samples. The profiler will also feature a sample carousel for storage. This concept provides the capability to collect all sample types, while ensuring a feasible landing procedure.

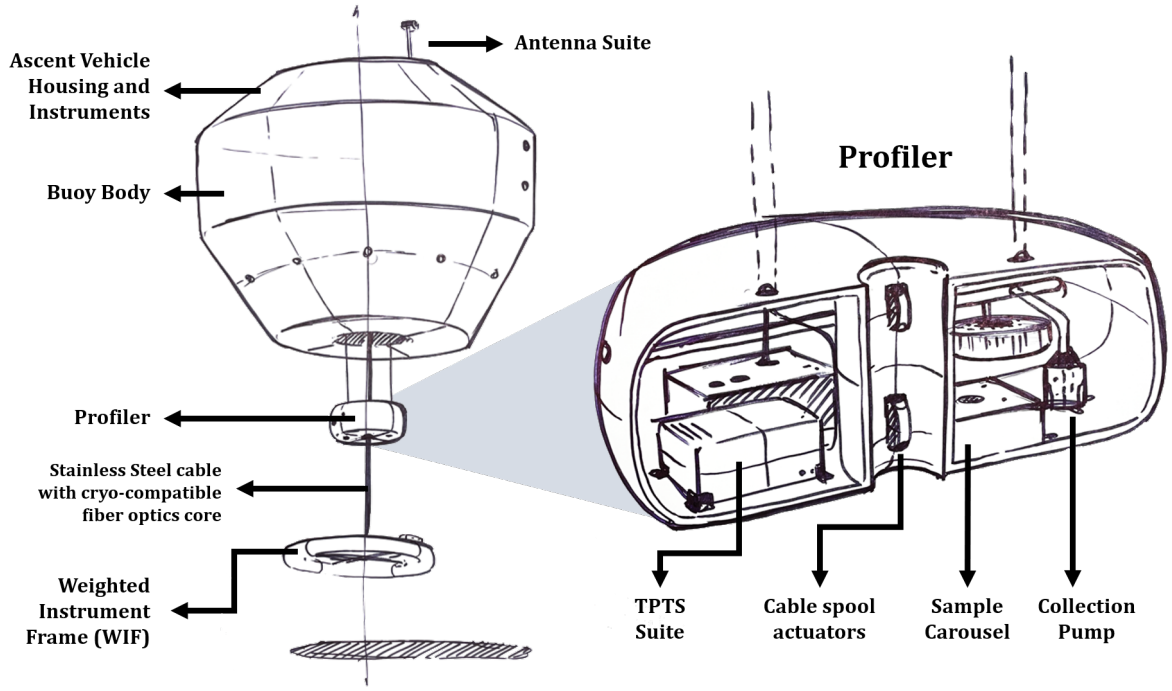

Fig. 7 Notional diagram of buoy with both WIF (below) and profiler (middle) deployed, showing a cross-sectional view of the profiler (right).

The selection of the ascent and orbiter concepts followed on from the selection of the lander. Having a single orbiter has several advantages including a single in-orbit rendezvous and leveraging heritage from both the Mars Sample Return [38] and Cassini missions. The orbiter features the xenon thrusters and instruments mentioned above, with a power subsystem based on the work from [39] which scales the Juno solar arrays for use at Titan. The orbiter requires 100 m^2 of solar arrays to produce 500 W at Titan, which even allowing for a 20% end of life deterioration, would be enough to power the spacecraft (see Section 4.D).

The ascent vehicle was designed to have as few single point failures as possible, ruling out deployable mechanisms and multi-agent launch systems such as balloons and rotor-lifted rockets were avoided. The final concept depicted in Fig.8 features a rocket-powered single stage to orbit vehicle, similar in nature to the Mars Ascent Vehicle [40] that relies on a liquid oxygen-liquid methane propellant, as preferred by both Landis and Donahue [41, 42]. The one moving part that remains in the system is the mechanism that will change the orientation of the ascent vehicle from horizontal while stowed on the buoy to vertical before launch. Moreover, the rocket length of 4.5 meters is what determines the minimum diameter of the buoy, which is limited at the other end by the maximum diameter of the aeroshell that would fit into the largest payload bay available of 9 meters on Starship. Given these constraints together with the buoyancy requirements, the buoy diameter is 5 m and the aeroshell is 8 m, making Starship the best viable launch vehicle option.

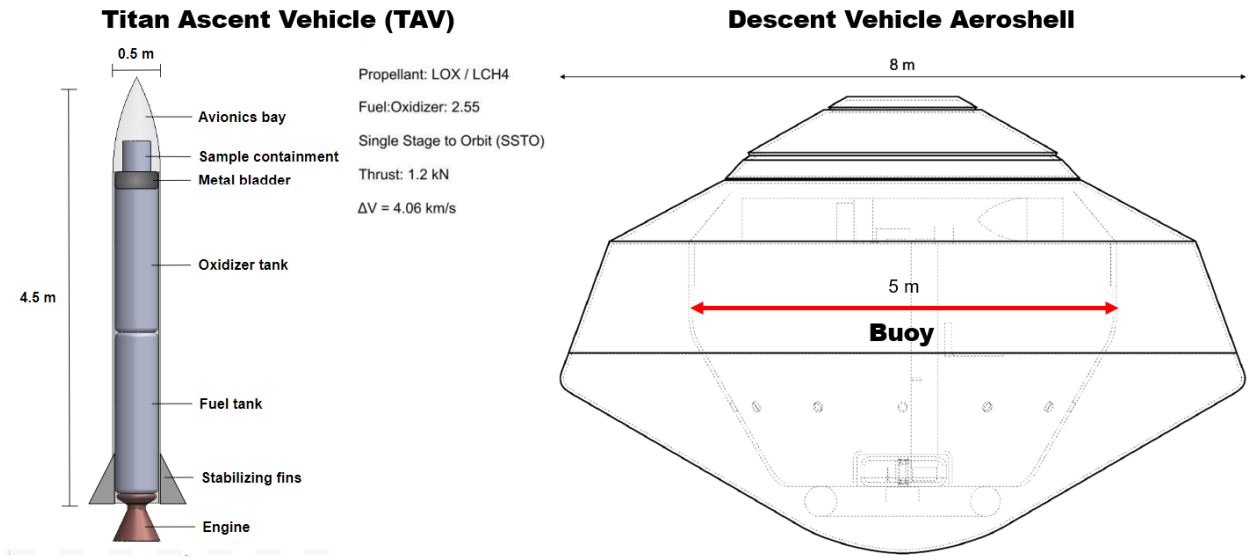

Fig. 8 Designs of the ascent vehicle (left) and the descent vehicle aeroshell (right).

The ideal Titan-Saturn mission takes place during Saturn's summer solstice in 2047 (the next summer solstice after the Dragonfly mission). This is when the poles normal to the equatorial plane of Saturn have the greatest tilt towards the Saturn-Sun inertial frame vector. In this window, there is maximum exposure to Earth for communications down/uplink. However, an analysis of possible Jupiter gravity-assists in Section IV.C indicates that the closest and most feasible time-of-arrival to Saturn is the year 2046. The arrival on Titan is a couple of years later, as the electric propulsion unit gradually reduces the trajectory energy and achieve the Titan Orbit Insertion as proposed by Strange et al [36]. Despite being 1 year after the Summer solstice, line-of-sight with Earth is still achieved as observed in 9.

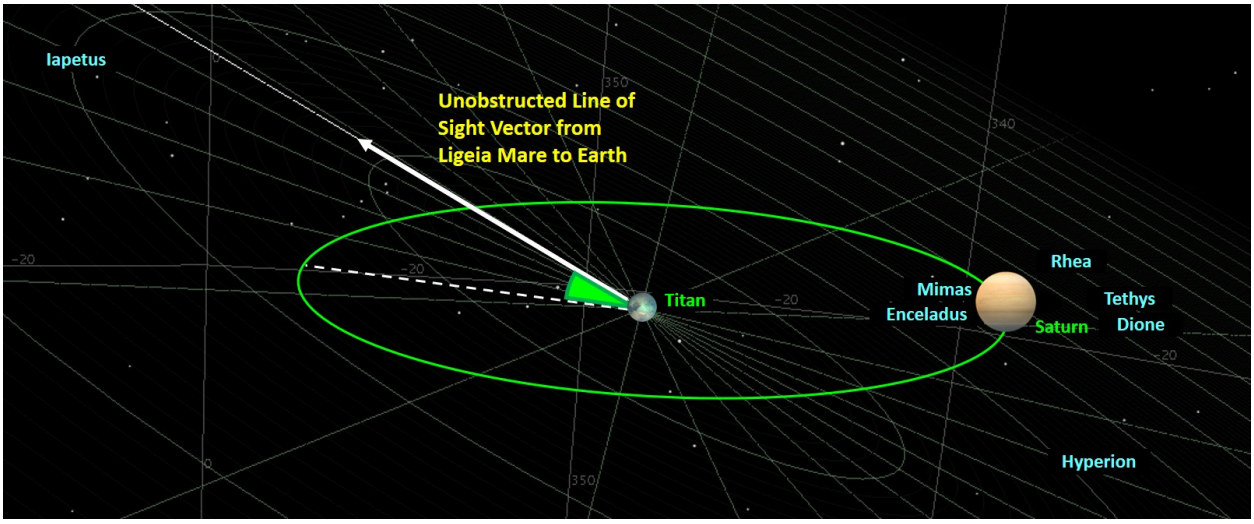

Fig. 9 Simulated orbit of Saturn about Titan origin in Jan 2048, imposed against the unobstructed line-of-sight vector between Ligeia Mare on Titan towards the Earth.

The *Az-El* plots in figs. 10a and 10b indicate that the view to Earth from Ligeia Mare is unobstructed throughout Year 2048, where the Ligeia Mare to Earth vector points at a typically shallow elevation, with an azimuth that cycles according to Titan's tidally locked period about Saturn (roughly every 16 days). The obliquity at low elevations leading to steeper atmospheric signal attenuation will also be accounted for in the link budget analysis in the full paper.

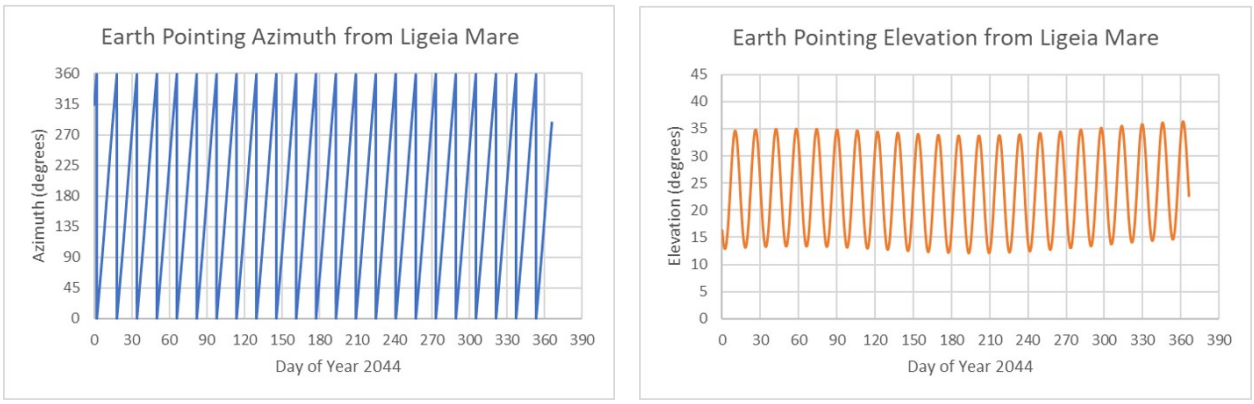

(a) **(b)**

Fig. 10 Visibility toward Earth from Ligeia Mare of a) unobstructed elevation and b) unobstructed azimuth for the year 2044.

B. Concept of Operations (ConOps)

1. From Earth to Titan

A SpaceX Starship equivalent launcher will be required. The choice of launch vehicle was largely determined by the payload (buoy) sizing, buoyancy requirements, and orbit subsystem sizing. The proposed initial launch date is October 2038, so as to leverage a Jupiter flyby in October 2040. The requirement is for the launcher to take the spacecraft into the transfer orbit with the required energy to reach Jupiter as $C_3 = 90.3\ km^2/s^2$, without prior flybys.

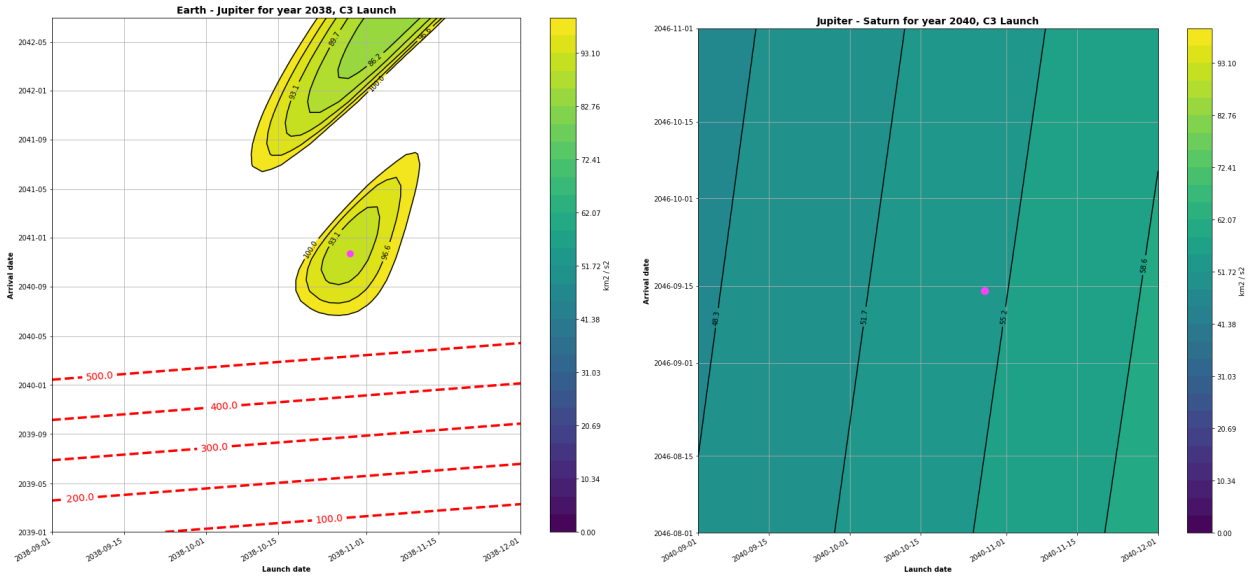

(a) **(b)**

Fig. 11 Trajectory window from a) Earth to the JGA, and b) Jupiter to the Saturn arrival.

After the gravity assist, the arrival into an orbit around Saturn is expected in 2046. Thus the total time of flight to reach Saturn for this preliminary mission design takes 7.89 years and a $\Delta V = 97\ m/s$ for the fly-by and the Saturn insertion. The feasible windows for the Jupiter Gravity Assist (JGA) and the Saturn Arrival are found using the porkchop plots in Fig. 11, where the pink dot represents the feasible date for the fly-by. The full trajectory from the Earth launch to Saturn is presented in Fig. 12.

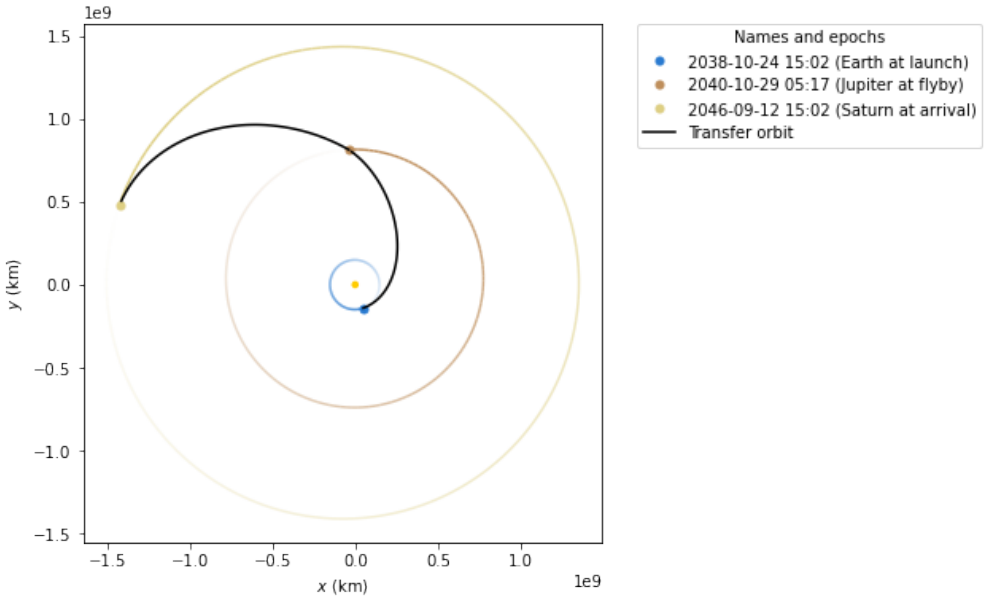

Fig. 12 Interplanetary trajectory from Earth to Saturn.

At the arrival to Saturn, the spacecraft will use solar electric propulsion (SEP) to fly a tour that reaches Titan with a low v-infinity as demonstrated by Strange et al. [43] and chemical propulsion to insert into an orbit around the Saturnian moon. The duration of the transfer will be of 2 years, therefore Titan will be reached on the year 2048.

The orbiter uses a dual resonant high gain antenna (HGA) operating in the Ka-band and X-band, with right-hand circular polarization (RHCP) polarization. It also has a dual resonant low gain antenna (LGA) operating in the X-band and S-band, also with RHCP polarization. The same dual-band RHCP LGA is also present on the lander. The transponders used for communication have legacy implementations in Cassini-Huygens [44], Mars Orbiter [45], Juno mission [46] and Titan Explorer [47]. A detailed trade study on use of antenna element and power amplifiers for Orbiter and Lander will be published in the full paper.

For communication systems from Earth to Titan, a high gain antenna will be used with low enough transmit power to generate a data rate around 50kbps for transmitting essential information about orbiter location and status. These are communicated to the 34 m and 70 m Deep Space Network (DSN) [48] antennas. Once Titan orbit insertion is complete, the X-band and S-band antennas on the orbiter are used to conduct atmospheric radiometry and IR measurements to estimate best time and landing locations pertaining to terrain and weather. When the lander separates from the orbiter, the lander LGA (S-band) and the orbiter LGA (S-band) are turned on. The S-band antenna has only a 6 dB gain and 74° beam width that allows the orbiter to perform a wide radiometric scan that makes it easier to find the lander.

2. On Titan

The landing takes place on the surface of Ligeia Mare via a splashdown with an entry velocity of about 6 m/s. Multiple constraints drove the design of the BOBII (Buoyant OBservation and In-situ Investigation) buoy. The length of the rocket without the nose cone, 4.5 m, sets a minimum bound on the diameter of the buoy. The diameter of the aeroshell, 8 m, dictates a maximum. Additionally, there needs to be margin between the buoy and the aeroshell to account for thermal insulation. Due to the nature of the methane lakes, even minor changes in temperature could significantly alter the composition of these liquids. At the same time, we must maintain near-room temperature conditions inside the buoy for the electronics. We therefore require a strong layer of thermal insulation between the outer shell of the buoy and the instrumentation inside to protect the lake from the thermal environment inside the buoy, leading to our multi-material buoy design. A simplified cross-section of this design is shown in Fig. 13. The entry velocity of ~6 m/s should be sufficiently slow enough for the buoy to stabilize itself and stay afloat as shown through a preliminary stability analysis in Sec. V.C. The rocket, electronics, communication suite, and some instrumentation systems are kept in the top section of the buoy to keep them thermally isolated from the liquid methane. The next layer down is made of aerogel, a

low-density, low-thermal conductivity material that isolates the lake from the heaters required to keep the electronics in the top section operational. A layer of high-density, low-thermal conductivity fiberglass laminate (G-10) exists below the profiler to provide thermal isolation for the profiler and to add weight to the bottom of the buoy for stability.

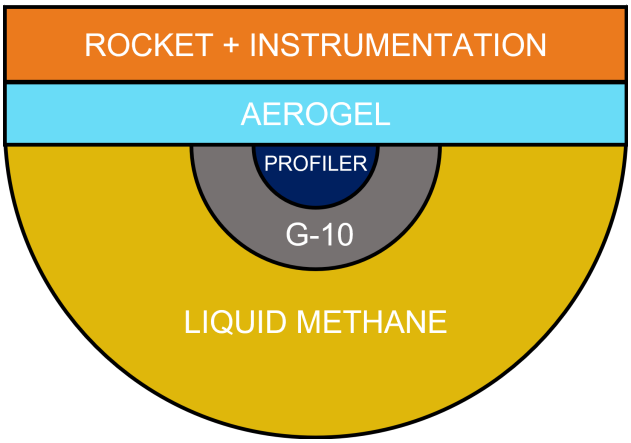

Fig. 13 Simplified cross-section view of the buoy used for center of mass and center of stability analyses with different material components shown.

After splashdown, there will be a stabilization period to allow the lake thermal environment around the buoy to stabilize. During this time, engineering checks shall be performed to ensure that all instruments are functioning properly. The sequence of operations occurring during the main mission lifetime are driven by the optimal science data collection order as shown in Fig. 14. On a high level, the goals in order of priority are:

1) Characterize liquid, atmosphere, and seafloor prior to collection,
2) Provide each sample collection with context of pre-collection, during collection, and post-collection measurements of the site,
3) Ensure sample collection is successful with mission control in the loop, and
4) Ensure all instruments are fully functional and operational.

Several 'idle' periods are allocated, in which all operations stop to preserve power, and the system waits to receive input from scientists and engineers in mission control. The slow, but regimented schedule ensures that all moving parts are operating as expected, with time to allow for corrections if needed. Due to the delays in communications and time to make decisions, each idle period is expected to last anywhere from 3 to 5 days at minimum power draw.

The sidescan sonar will image the seafloor morphology acoustically and the depth sounder will measure the depth to the bottom and to possibly detect layers and bubbles [49]. The Weighted Instrument Frame, externally docked to the bottom of the buoy, will then be released. Figure 7 shows the buoy with the WIF——the circular ring at the bottom——deployed. To control the descent of the WIF towards Ligeia Mare's seafloor, reservoirs on the WIF are filled in situ with liquid methane from the sea. The WIF houses a lens suite and a remote micro imager (RMI) that aids in characterizing various parameters of the surrounding seascape. The WIF acts as a weighted anchor to the buoy to prevent drift from tidal or wind-driven waves while collecting samples. The WIF is connected to the buoy with a stainless steel 316 hollow cable with cryogenic-compatible fiber optics [50] and electrical connections running through the cable to the WIF's instruments. After once again performing a systems check and relaying the status to Earth, a profiler will be lowered further down into the sea. The profiler can be raised and lowered by two cables, similar to WIF cables, that are attached to the buoy and are connected to a winch with a motor that controls its ascent/descent.

The profiler contains a carousel of containers for sample collection in the Ligeia Mare as well as a vacuum pump to enable the collection of samples. The sample collection carousel is similar to the Honeybee Robotics Sample Manipulation System for Perseverance [51]. The profiler also has thermocouples, pressure gauges, and turbidity sensors for in-situ data collection of the sea during sample collection. While the profiler is being lowered down for the first time along the WIF cable, the temperature, pressure, and turbidity sensors (TPTS) perform measurements of the surrounding environment.

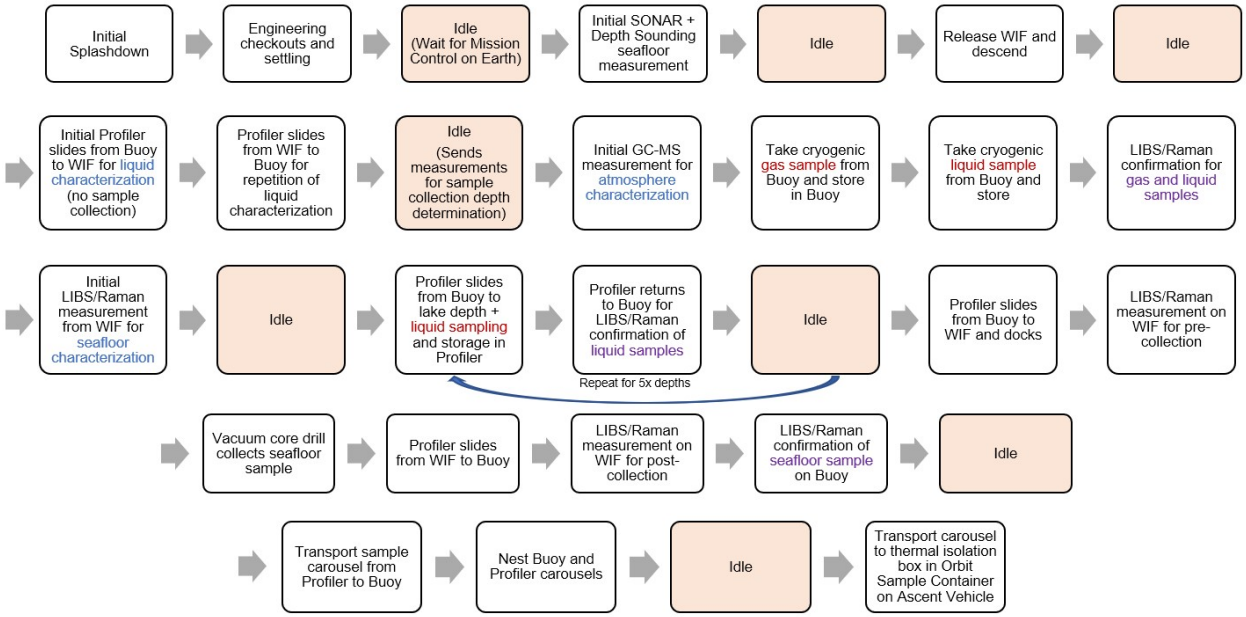

Fig. 14 Concept of operations for procedures on surface of Titan.

While the profiler collects liquid samples from below the surface of the lake and solid samples from the lake bed, the buoy has a small sample collection carousel with 7 sample collection tubes to collect gas samples from right above the Ligeia Mare surface and liquid samples from below the surface. The buoy sample collection carousel, similar to the one in the profiler, has sample collection tubes that are thermally isolated from one another to prevent heat transfer between different samples taken from different locations that might be at slightly different temperatures. Thermal isolation is maintained by having double walled SS 316 tubes with a vacuum in between the SS 316 layers to reduce thermal conductivity. The tube is hermetically sealed with a nylon interface to reduce the thermal conductivity of contacting surfaces. Sapphire windows, with a vacuum layer in between, are installed at the bottom of the tubes to enable sample analysis with the instruments located within the buoy. By doing this we both ensure that we are collecting the samples that we want and that we have duplicate information in case the samples cannot be returned to Earth. To prevent thermal shock to the samples being collected, the sample collector tube is brought to the temperature of the samples in advance by placing a pre-cooling coil inside the tube (see fig. 15). Fluid from the sample collection area of Titan's sea is passed through the coil via vacuum pump, bringing the coil to the temperature of the region of sample collection. The inside of the collector tube is then brought to the same temperature via conduction to the interior walls. The coolant fluid from the coil is exhausted further away from the sample collection site to minimize thermal transfer. After the sample collector tube has been cooled, the actual sample is collected into the tube by redirecting the flow of the fluid into the tube.

Once the samples have been collected, Raman spectroscopy and LIBS measurements are performed on the samples to verify successful collection. To collect the solid lake bed samples, the profiler is lowered along the cable and docks to the WIF anchored to the seafloor. A seafloor characterization measurement is performed by Raman spectroscopy and LIBS. To collect a solid sample from the seafloor, a core drill extends from the profiler and drills into the seafloor. The solid sample, along with some liquid, is collected by a vacuum pump before the liquid is then filtered out, the solid sample is placed in the profiler sample collection tubes, and the tubes hermetically sealed.

The profiler sample collection carousel is transported through the buoy on tracks that end at the nosecone of the ascent vehicle. Before being transported to the ascent vehicle, the buoy sample collector carousel is nested into the profiler sample collector carousel. The entire carousel system is then transported to the ascent vehicle which has a thermally-isolated container in which the carousel is placed and hermetically sealed. This additional thermal isolation provides additional protection against heat and keeps the samples within 1 K of their collection temperature, particularly during reentry into Earth.

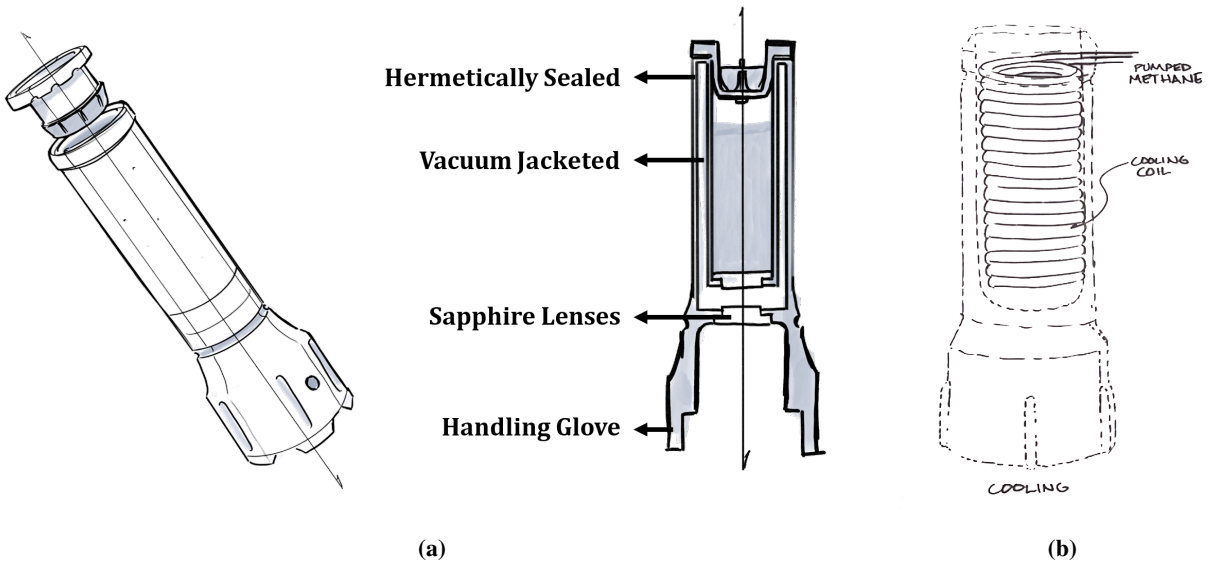

Fig. 15 Sample collection tube design with a) parts identified and b) thermal considerations.

Once the lander arrives on Ligeia Mare, the communication link is re-established from orbiter to the lander. The orbiter trajectory and speed results in roughly 2 hours of period in one Earth day when the orbiter is in sight of the Lander. Since only steering up to +/- 60° from boresight is possible, the entire horizon cannot be scanned by the phased array on the lander to establish a lock with the orbiter and vice-versa. Because of this, the effective time that the lander can track the orbiter reduces to about 50 minutes. After Lander-Orbiter lock , lander uses its X-band phased array antenna to track the orbiter and send telemetry. It is estimated that the payloads generate roughly 1200 Mb of data per day. Using the X-band telemetry from the lander to the X-band LGA of the orbiter, data can be sent at sufficiently fast speeds to ensure that all data is sent in 13 minutes. The detailed telemetry performance will be shown using the link budget analysis in the full paper. While the orbiter is not in communication with the lander, it uses its HGA K-band or X-band systems to transmit the data to Earth DSN. 70 m stations are used for X-band telemetry and 34 m stations are used for Ka-band telemetry. The Earth can send return uplink data to the Orbiter and lander through the same 34 m and 70 m stations for routine maintenance and software updates. After the mission is deemed completed by sending specific codes using Earth DSN uplink, the rocket prepares for ascent. Once the rocket has achieved lift-off, the S-band LGA about the lander and orbiter are again activated for tracking sample drop-off. On completion of the sample drop-off process, the orbiter prepares for rendezvous and collects the samples to bring them back to Earth.

3. From Titan to Earth

Upon sample insertion into low Titan orbit, the rendezvous operation will commence. A notional sketch of the orbiter in rendezvous phase is in Fig 19, and full details of the rendezvous are expounded in Section V.E. After rendezvous, we begin the return trajectory. Invariant manifolds of the Saturn-Titan Circular Restricted 3 Body Problem are natural transport mechanisms that can be used to design a low ΔV trajectory. The main idea behind the return trajectory design is to use these structures to transfer the spacecraft from the orbit around Titan to a resonant orbit around Saturn. Resonant orbits can be described with the ratio $n : m$, where, for example, n is the number of revolutions of Titan around Saturn, and m is the number of revolutions of the spacecraft around Saturn [52]. By using a resonant orbit, we can leverage successive gravity assists with Titan and/or other moons, to increase the semi-major axis of the orbit and gain sufficient energy to escape the system. This approach follows the step of the trajectory proposed by Galwik et al [53] and by Vaquero [54] for the inverse problem, e.g. transfer the spacecraft from an orbit around Saturn to an orbit around Titan.

The final trajectory will be composed by 4 main parts. First, the spacecraft will start the Titan orbit altitude raise phase using electric propulsion. This choice is motivated by limited amount of chemical propulsion on board of the return module. The chemical propellant is preserved in this phase, such that it can be used for the interplanetary trajectory maneuvers. The raising maneuver will target an invariant manifolds that connects the Titan region to a resonant orbit

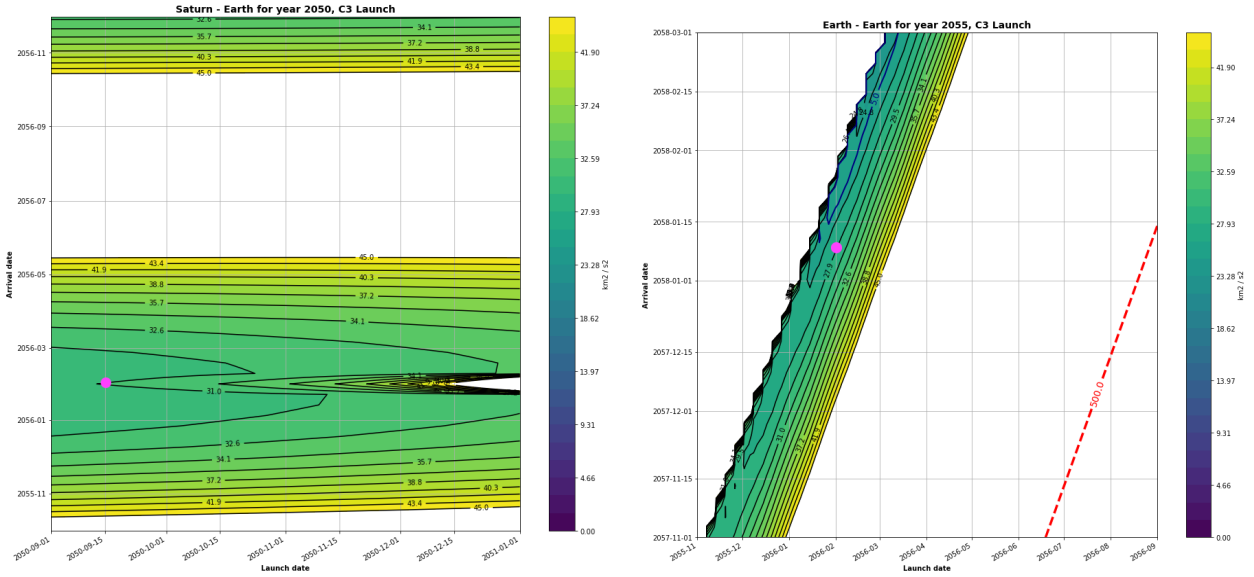

(a) **(b)**

Fig. 16 Trajectory window from a) Saturn to the EGA, and b) EGA to the Earth arrival.

around Saturn. The manifold insertion maneuver can be performed using low thrust propulsion. Once the resonant orbit is reached, the spacecraft will perform a sequence of gravity assists, where impulsive ΔV can be used to correct the outgoing trajectory. The estimated duration of these phases is approximately 1 year. This phase is concluded when the spacecraft reaches the energy value to insert an interplanetary transfer and leave the Saturn system.

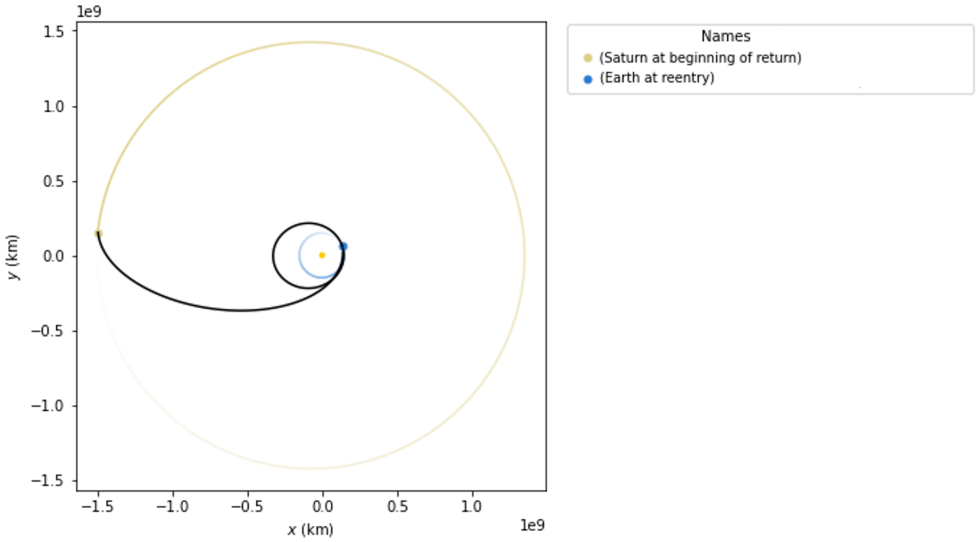

Fig. 17 Example of interplanetary return trajectory from Saturn to Earth

To mitigate risk of damage, thermal failure, and contamination to the samples, without compromising too heavily on ΔV, the return trajectory will target the Earth to perform a fly-by that inserts the orbiter in a 2:1 resonant orbit with the Earth. One or two additional fly-bys with the Earth will follow, to decrease the orbiter speed and target the Earth SOI for re-entry. Additionally, the v_∞ leveraging technique [55] can be used at the pericenter of each revolution of the resonant orbits to decrease the orbit energy to reach a favorable ΔV for the Earth capture. An example of the final interplanetary trajectory for the return is shown in Fig. 17. The ideal dates are selected using the porkchop plots in Fig. 16, where the

first shown the Saturn-Earth leg between 2050 and 2056, the second targets the resonant orbit with the Earth from 2056 to 2058. The pink dots represent the possible dates for the insertion and the gravity assist respectively.

This scenario represents a possible solution for the return trajectory, however additional investigations are necessary to compute the exact transfer segments and their cost in terms of ΔV.

C. Overview of Budgets

The overall mass, ΔV, and power budget for the orbiter, lander and ascent vehicle are summarized here. More information on each budget is presented in Section 5 which discusses the detailed design of each mission element.

1. Total System Mass Budget

The approximation for the orbiter and lander EDL system mass is based on the Mars Science Laboratory [30] and Cassini [20]. The mass of the buoy results from floating and stability requirements, while the ascent vehicle is sized based on the delta V needed to insert the samples into Titan's orbit as well as on the Mars Ascent Vehicle. The system mass is summarized below in Table 1.

Table 1 Mission mass budget

Element	Mass (tonnes)
Orbiter Dry Mass	1.02
Orbiter Chemical Propellant	1.6
EDL System	2.6
Buoy (landed mass)	4.9
Ascent Vehicle	0.65
Total	10.75

2. Total System Power Budget

In terms of power requirements, the power budgets for the orbiter and the lander are listed in Table 2. The 100 m^2 of solar panels on the orbiter (see depiction in Fig. 19) can produce enough power at Titan for the operation of the orbiter. The 1380 Ahr battery system on the lander provides energy for 200 hours of high-power science operation which gives a 50 day mission life with 40% margin. Out of those 200 hours, 77 are spent moving the profiler, 10 taking measurements with the LIBS/Raman instruments, 100 communicating the data and 5 mapping the sea floor. The rest of the time is spent in idle mode where the OBC is the main power consumer.

Table 2 Mission power budget

Element	Power Budget
Orbiter	Communication - 250 W Instruments - 68 W Heaters - 50 W OBC - 10 W
Lander	Profiler Traversal - 77.5 W Instruments - 90 W Communication - 60 W Floor Mapping - 37 W Idle - 10 W
Total	Orbiter - 378 W Lander - 22.6 kWhr

3. Total System ΔV Budget

Trajectory simulations and ΔV estimations were performed using Poliastro [56]. Similar trajectory design studies for a Titan mission have been done by Strange [36] and Vaquero [54]. Due to the system sizing, we require that the initial insertion into Jupiter be conducted by the launch vehicle rather than the orbiter's NEXT propulsion units. A 25% margin was used for the budgeted ΔV over the computed ΔV. Pre-descent ΔV computations in Table 3 include the dry mass of the entire EDL system (7532kg), while post-descent ΔV computations in Table **??**

Table 3 Earth to Saturn (Pre-Descent): ΔV Budget (km/s)

	Earth to Jupiter	Jupiter Gravity Assist	Saturn Insertion	**Subtotal**
Propulsion	Launcher	Chemical	Chemical	
Computed ΔV (km/s)	6.760	0.006	0.091	**0.097**
Budgeted ΔV (km/s)	6.900	0.09	0.137	**0.138**
Propellant Mass (kg)	-	221.821	327.546	**549.367**

Table 4 Titan Orbit Operations (Post-Descent): ΔV Budget (km/s)

	Titan Insertion	Titan Aerobraking	Orbit Circularizing	**Subtotal**
Propulsion	Electric	Electric	Electric	**-**
Computed ΔV (km/s)	0.388	0.079	0.085	0.552
Budgeted ΔV (km/s)	0.485	0.099	0.106	**0.690**
Propellant Mass (kg)	14.353	2.909	3.107	**20.369**

Table 5 Saturn to Earth: ΔV Budget (km/s)

	Titan Orbit Raise	Saturn Resonance	Saturn to Earth Capture	**Subtotal**
Propulsion	Electric	Electric	Electric	**-**
Computed ΔV (km/s)	0.040	0.100	5.100	**5.240**
Budgeted ΔV (km/s)	0.050	0.125	6.375	**6.550**
Propellant Mass (kg)	1.463	3.649	172.06	**177.172**

4. Expected Financial Budget

The mission cost was divided between the orbiter, the ascent vehicle and the lander. The orbiter was approximated to cost around $600 million from the USCM8 non-recurring subsystem CERs based on the 2010 financial year [57], while the ascent vehicle was based on the MAV cost [58] and will be around $318 million. The lander features several complex subsystems and is predicted to involve a high development cost which is difficult to predict. However, the Cassini-Huygens mission was taken as a reference to estimate the total mission cost. The Cassini-Huygens mission was around $3.3 billion with half the take-off mass and a lander which is a tenth of the mass compared to the current system. As a result, the lander can cost around twice as much as the entire Cassini-Huygens mission, around $6.5 billion, raising the total mission cost to $7.4 billion, making this a Flagship-class mission.

V. System Sizing and Design

A. The Orbiter

The orbiter plays three critical roles. First, as the primary transport for the descent vehicle; second, to provide pre-descent ops support via an in-situ surface imaging and wind profiling of Titan so as to characterize the circular error probable of

the landing ellipse centered on Ligeia Mare; third, as a return vehicle to rendezvous with the collected samples cached in the ascent vehicle. Design considerations for housing the lander were modelled after the Mars Science Laboratory, while design considerations for instrumentation in pre-ops descent were inspired by the Cassini instruments and bus. A notional diagram of the basic orbiter design is given in Fig 18 and a notional sketch of the key elements necessary for relative navigation to the sample and sample rendezvous is given in Fig 19.

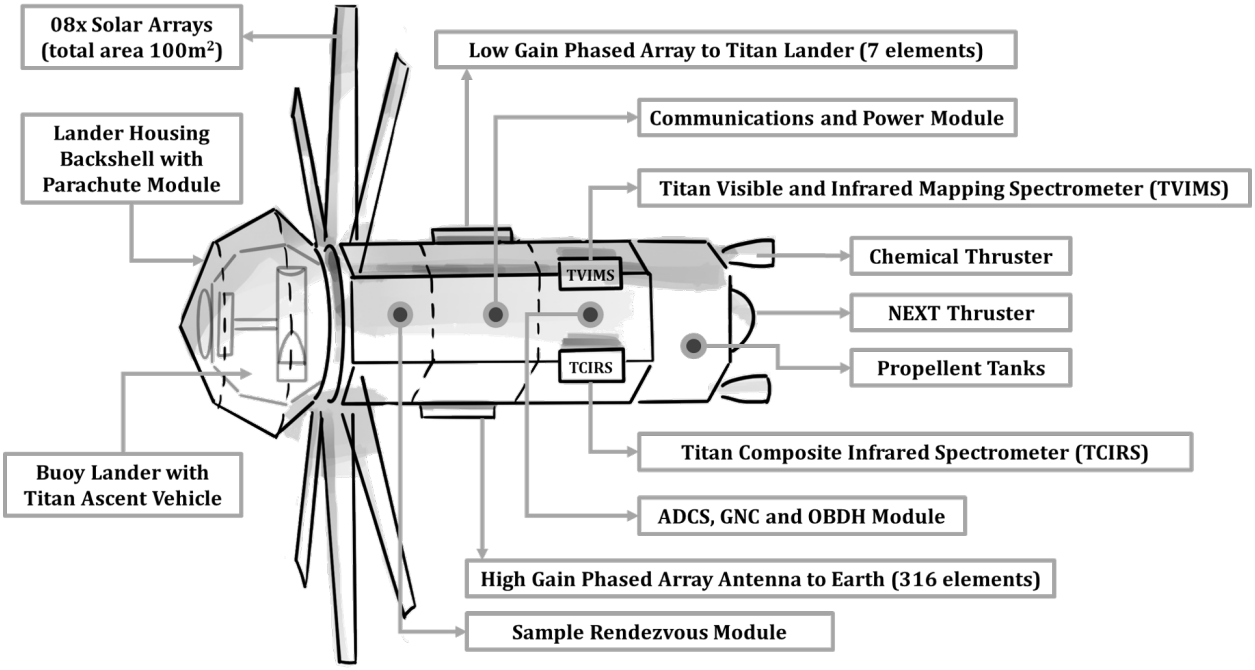

Fig. 18 Notional sketch of orbiter in pre-descent ops with necessary subsystems and instruments.

1. Orbiter Sensors and Instruments

Adapting from Cassini, two instruments are necessary for a successful landing. First, the Titan Visible and Infrared Mapping Spectrometer (TVIMS) adapted from Cassini's VIMS [37], provides surface imaging for orbit determination and landing ellipse characterization. It has imaged Titan's lakes successfully on Cassini. TVIMS is preferred over other computationally intensive (and typically post-processed) imaging instruments of Cassini such as synthetic aperture radar. VIMS provides the immediacy of images necessary for time-critical descent operations. Second, the Titan Composite Infrared Spectrometer (TCIRS), adapted from Cassini's CIRS [37], is used for wind profiling and thus descent risk assessment. It has proved to measure wind down to Titan's stratosphere [9]. Additionally, in the post-descent phase, where the lander housing and backshell has left the orbiter bus, the exposed rendezvous module reveals the capture funnel and two additional sensors (a camera and a mmWave radar for range), as sketched in Fig 19. The sensors provide measurements for the relative navigation filter to estimate relative states between the orbiter and the sample capsule during rendezvous phase. This is expounded in Section V.E.

2. Orbiter Power Budget

The critical considerations are the communications, instrumentation, computing (OBDH) and heating subsystems. Communications consumes $250W$ in the most expensive case from Titan to Earth (see Section V.F. The instruments TVIMS and TCIRS consume $68W$ in total during simultaneous use. The heating subsystems consume $50W$, which can be reduced with lightweight radio-isotope units [59]. The on-board computer consumes $10W$. Without including the 6.9kW NEXT thrusters, the operating power in low Titan orbit $\approx 378W$. For power generation, a comparison was done between solar power and radio-isotope thermal generators (RTG). Pure solar-based power was chosen, due to its relative simplicity in implementation as compared to RTGs which would necessitate installing a complex thermal and

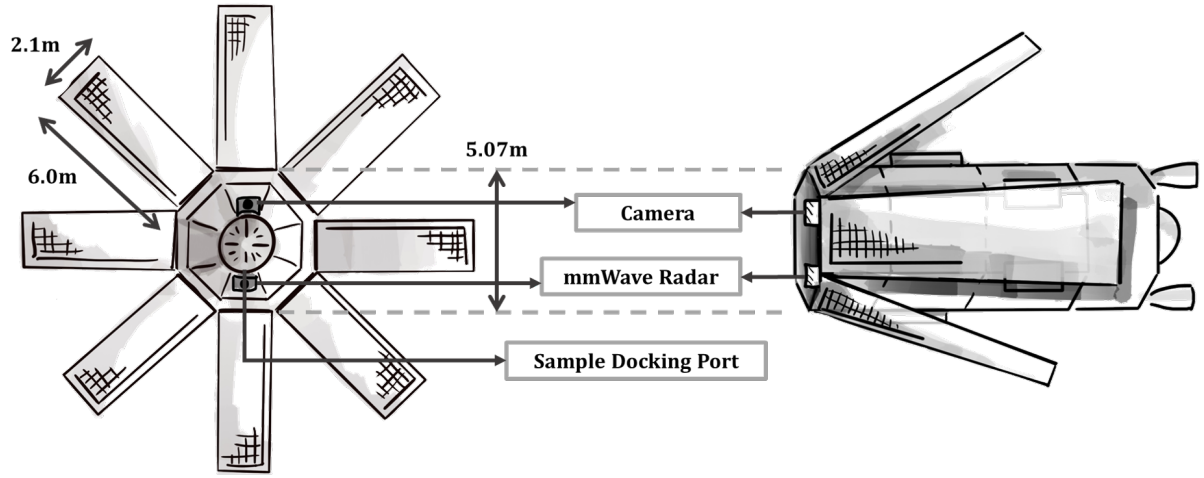

Fig. 19 Notional sketch of orbiter with rendezvous capsule exposed (front view on left, side view on right).

fluidic re-distribution system. For solar power, despite inverse square law losses, a power intensity of $15W/m^2$ is still achievable at Saturnian distances. This value was modelled by scaling the solar power generation of the Juno spacecraft at Saturn [39]. Thus, with 30% efficiency and designing the effective normal solar cell area $\approx 100m^2$, the orbiter can produce $500W$ at low Titan orbit, which meets power requirements for necessary operations.

3. Orbiter Mass and ΔV Budget

Preliminary masses of subsystems were found by iterative estimations from linear regression using previous interplanetary space missions such as Cassini-Huygens [37], Juno [46], and the Mars Science Laboratory [45]. The orbiter-only dry mass breakdown is given in Table 6. The dry mass figures already account for 10% margin. Table 6 does not include the total mass of the landing buoy with backshell $\approx$ 7532kg and the total propellant. A comprehensive breakdown of the lander system mass is expounded upon in Section V.C. Propellant wet masses are tabulated in Tables 3, 4, and 5.

Table 6 Dry mass breakdown of the orbiter (without the lander and backshell).

	Thrusters	Structure	Power	Instruments	ADCS	OBDH	Comms	Thermal	**Subtotal**
Mass (kg)	300.0	200.0	250.0	80.0	64.4	53.7	40.0	32.2	**1020.3**
Percentage	29.4%	24.5%	19.6%	7.84%	6.31%	5.26%	3.92%	3.16%	**100**%

First, the mission needs a high specific impulse electric propulsion thruster for Titan-Saturn system maneuvers with only low-thrust requirements so as to minimize wet mass. Second, a chemical thruster with a larger thrust, at the expense of a lower specific impulse, is necessary for gravity assists correction maneuvers. For electric propulsion, the NASA Evolutionary Xenon Thruster (NEXT) was a perfect candidate, given its remarkable $I_{SP} = 4170s$, thrust of 237mN, and deep-space heritage with the success of DART [60]. For chemical propulsion, a hydrazine-based thruster similar to Cassini's was assumed, with $I_{SP} = 300s$ and thrust of 2N. Propellant of Xenon (electric) and Hydrazine (chemical) were estimated using the rocket equation in Table **??**. The lander mass $\approx$ 7532kg was included during the journey to Titan, but discarded for the return journey to Earth,

4. Orbiter Guidance, Navigation and Control

As standard devices for spacecraft guidance, navigation and control, the TURTLE orbiter will be equipped with a star tracker and an inertial reference unit for attitude determination. Reaction wheels stabilize the attitude. Absolute orbit determination can be achieved coarsely using terrain relative navigation of Titan, aided by the DSN/USN network. Relative orbit determination, particularly during sample rendezvous and capture relies on a radar sensor and monocular camera for azimuth, elevation, and range measurements for relative state estimation.

5. Orbit Insertion and Selection

The initial orbit upon Titan insertion is expected to be highly elliptical, as expounded in IV.B.1. Circularizing the orbit can be made efficient using a hybrid orbit maintenance strategy that exploits Titan's thick atmosphere for aerobraking in parallel with propulsion as seen in Figure. A closed-form computation of the decay rate as derived in [61] allows for efficient orbit maintenance planning, subject to the accuracy of knowledge of Titan's atmospheric densities. In the final selection of the operating orbit, the most obvious design factor is an orbit inclination that matches the latitude of Ligeia Mare. This is at 79.5°.

In the selection of altitudes, the first orbit design factor was to balance the gain in signal-to-noise ratio of the orbiter instruments at lower altitudes, against the cost of requiring greater ΔV to escape Titan's gravity well during the return trip, and the costs of orbit maintenance due to Titan's thick atmospheric drag at lower altitudes. The second design factor was to choose an altitude that was reachable by the ascent stage vehicle ferrying the samples, which is elaborated on in Section V.D. The third and final design factor was to select an altitude such that a repeated ground track over Ligeia Mare can be established with reasonable re-visit frequency. A reasonable range of altitudes balancing all three design factors are within 1400 to 1600 km. A range of possible repeat ground tracks, together with their preliminary frozen eccentricity values at each altitude are tabulated in Table 7. This analysis uses J2 = 3.3089E-05 and J3 = -1.79E-07 from the results of Cassini's dedicated gravimetric data-collection passes in [62].

Table 7 Orbit repeat ground track metrics between 1400 to 1600 km altitude.

Altitude (km)	1421.2	1453.9	1487.5	1521.7	1556.6	1592.3
Orbits per Repeat	82	81	80	79	78	77
Frozen Eccentricity	0.001735	0.001700	0.001686	0.001671	0.001658	0.001643

The final choice of elements were derived by iterating between the three aforementioned design factors until a satisfactory compromise can be made between them. They are tabulated below in Table 8.

Table 8 Operating Orbital (Keplerian) Elements.

Epoch (UTC)	Altitude (km)	a (km)	e	i (°)	ω (°)	Ω (°)	ν (°)
01 Sept 2048 00:00:00	1521.7	4096.43	0.001671	79.5	90.0	0.0	0.0

From the analysis of the ground track, Ligeia Mare will be visited 2.5 times per Earth day for an average duration of 36 minutes per passage, ensuring proper communication in uplink and downlink with the orbiter. A dedicated analysis on communications is found in V.F.

B. Entry, Descent and Landing

After selection of a ballistic 'splashdown' scenario for entry, descent and landing, there were a number of considerations to consider in the design of the descent vehicle and parachute. The descent vehicle aeroshell and backshell have to be sized to house our lander, as well as avoiding any peak heating or total heat load constraints. Additionally, the instruments onboard our final lander are rated to 10 g's, so deceleration values during descent must not exceed this value.

The descent vehicle (the heatshield and aeroshell, and the backshell and parachutes) were approximately sized based primarily on the required dimensions of the lander, to support all of the instrumentation, ballast mass and ensure the desired mass distribution and buoyancy in the water. Assuming a launch on a SpaceX Starship, with a payload fairing of 9m diameter, an 8 m diameter aeroshell was selected. The aeroshell is a 70^o spherecone based on the shape shown in Fig. 20. Given the higher density atmosphere, the nose is blunted (high nose radius) so that the stagnation point will not move off of the nose. In addition, the depth of the aeroshell is increased compared to the Dragonfly and Perserverance aeroshells to accommodate for the large payload size.

The ballistic coefficient β, an important factor in calculating EDL characteristics for the descent vehicle, was calculated using the following equations:

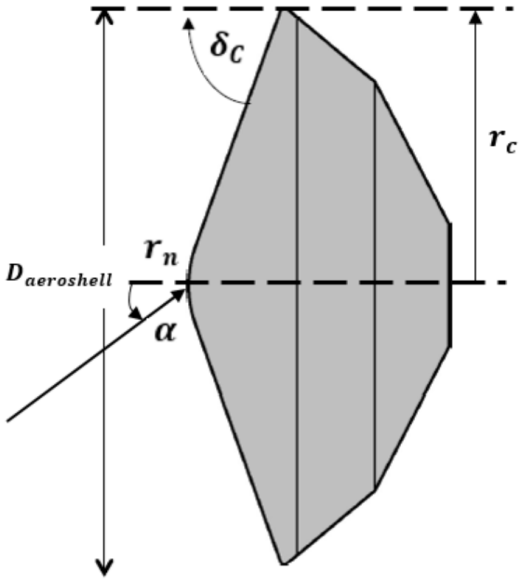

Fig. 20 Spherecone Aeroshell Configuration

$$b = \frac{r_n}{r_c} C_L = C_N \cos\alpha - C_A \sin\alpha \tag{1}$$

$$C_D = C_A \cos\alpha + C_N \sin\alpha \tag{2}$$

$$C_N = [1 - b^2 \cos\delta_c] \cos^2\delta_c \sin 2\alpha \tag{3}$$

$$C_A = b^2 \left[1 - \sin^4\delta_c\right] + \left[2\sin^2\delta_c \cos^2\alpha + \cos^2\delta_c \sin^2\alpha\right] \left[1 - b^2 \cos^2\delta_c\right] \tag{4}$$

$$\beta = \frac{m}{C_D A_{ref}} \tag{5}$$

where m is the total entry mass of the vehicle (i.e. the landed mass plus the EDL system), C_D is the drag coefficient, and A_{ref} is the projected reference area, in this case calculated from the base radii of the aeroshell. Our descent vehicle has a ballistic coefficient of $\beta = 84.5$ kg/m^2. The aeroshell mass was estimated based on the EDL efficiency number [63], i.e. the ratio of the entry mass to the landed useful mass. The EDL efficiency for the Mars Exploration Rovers (MERS) was used as a baseline estimate, as the MERS EDL scenario is similar to the proposed Titan EDL scenario (ballistic entry with no attitude control or retropropulsive braking, and two parachutes). Based on a MERS EDL efficiency of 1.54, and a landed buoy mass of 4896 kg, the descent vehicle (parachutes, thermal protection system, aeroshell and backshell) have a mass of 2636kg, for a total entry mass of 7532 kg. The aeroshell with the stowed buoy lander is shown in Fig. 21.

For much of the analysis of the EDL scenario, a set of simulations of Titan EDL scenarios completed by the Space Systems Design Laboratory at the Georgia Institute of Technology was used [64]. This analysis is shown in the subsequent subsections.

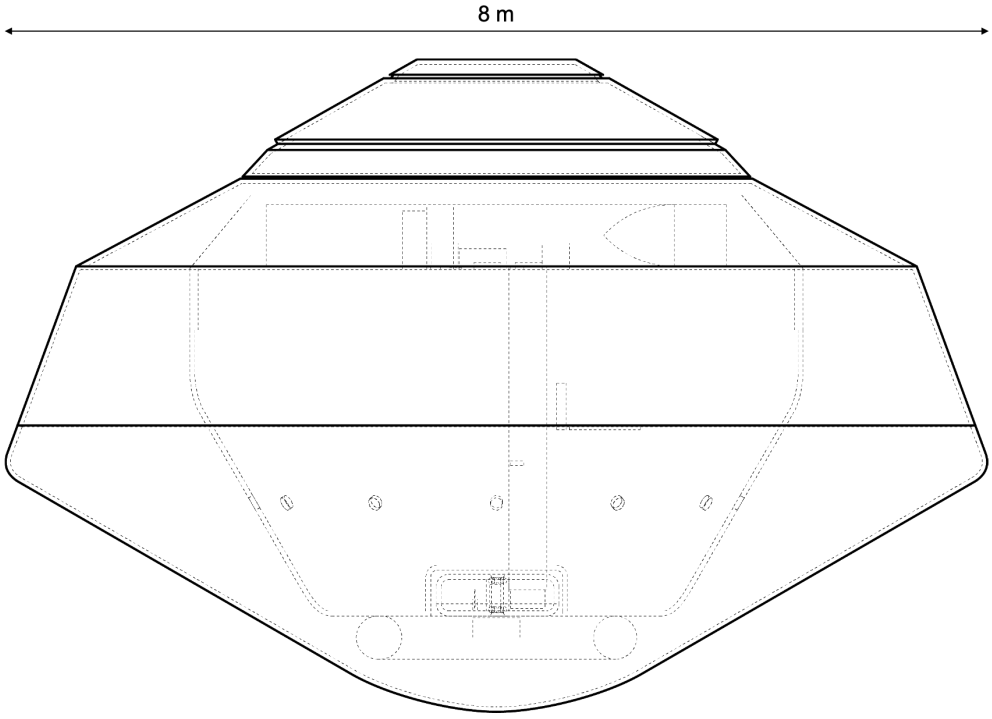

Fig. 21 70^o spherecone aeroshell, with stowed buoy lander

1. Entry

The lander will enter the Titan atmosphere from orbit (rather than direct entry used by the Huygens probe and proposed by the Dragonfly mission) at the atmospheric interface of 1270 km after a retropropulsive burn in its polar orbit at 1500km. Orbiting at this altitude the entry velocity will be 1.5 km/s. As stated above, the entry will be a ballistic trajectory and thus the vehicle will have a 0^o angle of attack. Prior to de-orbit and atmospheric entry, the orbiter will map the northern polar region with IR, to identify a landing site on Ligeria Mare. Given the large size of Ligeria Mare and the predicted size of our landing ellipse (see below), orbiting IR provides sufficient resolution for the calculation of landing solution. Characterization of the atmospheric winds will also be done prior to de-orbit using instrumentation onboard the orbiter. This is will enable an updated estimate on landing ellipse based on the measured wind speeds over the northern polar region, and consequently final selection of the atmospheric entry point and entry vector.

The entry flight path angle is selected based on our ballistic coefficient and the allowable loads for the vehicle. Given that our instruments should not exceed 10 g's, and β = 84, our entry flight path angle will be between -55^o and -50^o.

Given our ballistic coefficient and assuming an entry flight path angle of -55^o, the descent vehicle will experience an integrated heat load of 2500 J/cm^2, as seen in Fig. 23a, and a peak heat rate of approximately 55 W/cm^2. These values are far lower than those experienced by Mars Pathfinder or the Mars Exploration Rovers [65]. Consequently, the thermal protection system (TPS) will use the state of the art PICA ablative shield material, which should be more than sufficient to provide thermal shielding to our lander [66].

2. Descent

The descent vehicle deploys its first parachute when the trigger velocity is reached, which occurs after peak deceleration of 10g. After some time, the second main parachute is deployed, further slowing down the aeroshell and payload. This will likely occur below the altitude of the high winds in Titan's atmosphere, which decreases the horizontal displacement of the lander, however this specific velocity will be determined after the atmospheric winds have been characterized by the orbiter. This is based on a steady descent for in situ atmospheric measurements and reducing points of failure. The diameter ratio η_D of the descent vehicle is described in the equation below:

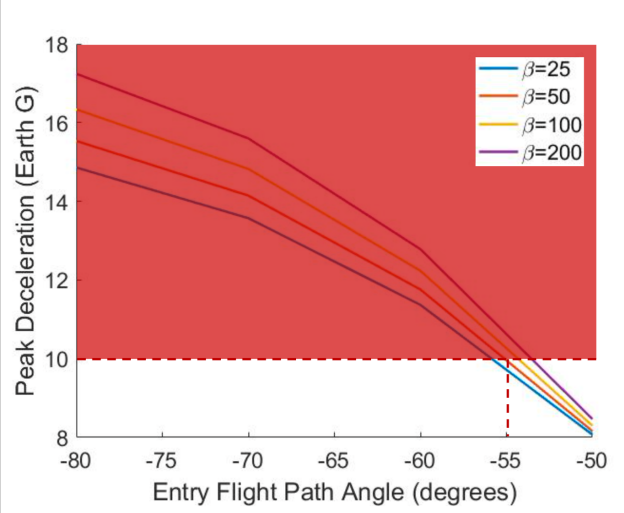

Fig. 22 Flight path angle vs peak deceleration

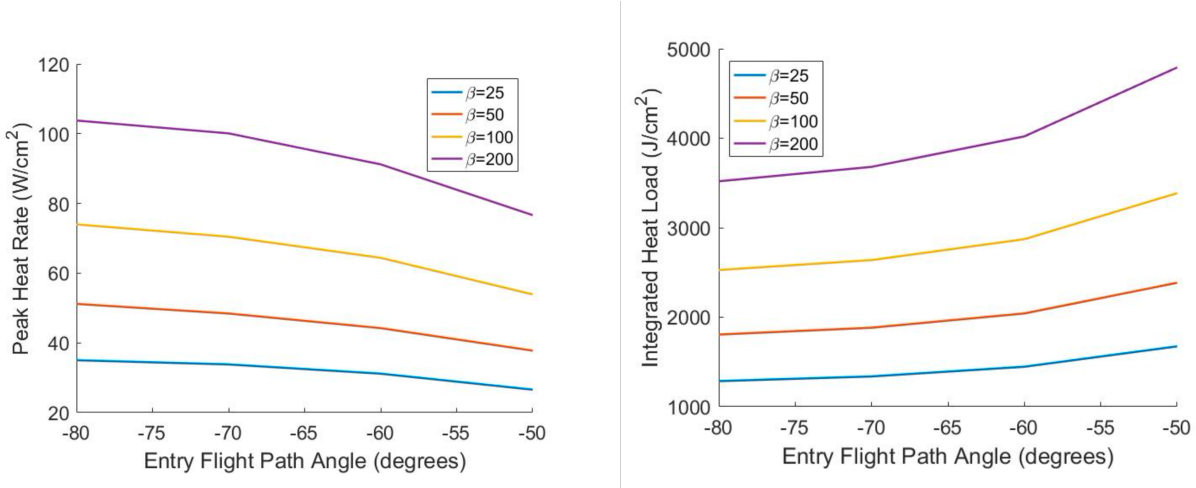

(a) Integrated Heat Load vs Entry Flight Path Angle for different Ballistic Coefficients [64]

(b) Peak Heat Rate vs Entry Flight Path Angle for different Ballistic Coefficients [64]

Fig. 23 Heat load and heat rate for differen Ballistic Coefficients

$$\eta_D = \frac{D_{parachute}}{D_{aeroshell}} \tag{6}$$

This will be used in the calculations of the final descent parameters.

3. Landing

The landing takes place on the surface of Ligaeia Mare. This will be a splashdown with an entry velocity of about 6 m/s. This should be sufficiently slow enough for the buoy to stabilize itself and stay afloat, based on the buoyancy calculations in the surface operations portion of this report. Based on analysis done by [64] and as seen in Fig. 24, our ballistic coefficient and a sufficiently high parachute diameter ratio should ensure our impact speed is approximately 6 m/s.

The landing ellipse is based on possible ratios of parachute diameter as characterized by Figures 25a and 25b. These figures are from analysis done by [64], where for an orbital entry speed of 4 km/s, and different ballistic coefficients, the

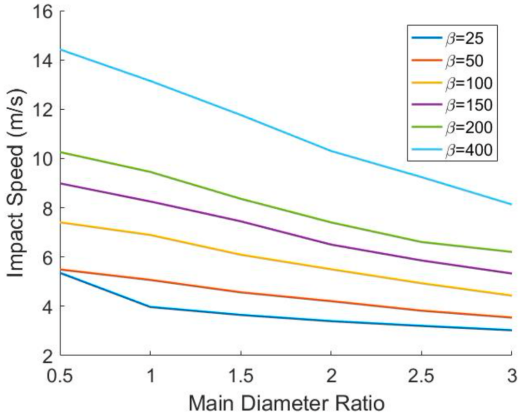

Fig. 24 Impact speed vs Diameter Ratio for 4 km/s entry velocity [64]

possible crossrange and downrange errors in landing site were calculated based on winds at the northern polar region. From these plots, with our ballistic coefficient, we are looking at a maximum landing ellipse of 125 x 175 km, well within the confines of Ligeria Mare.

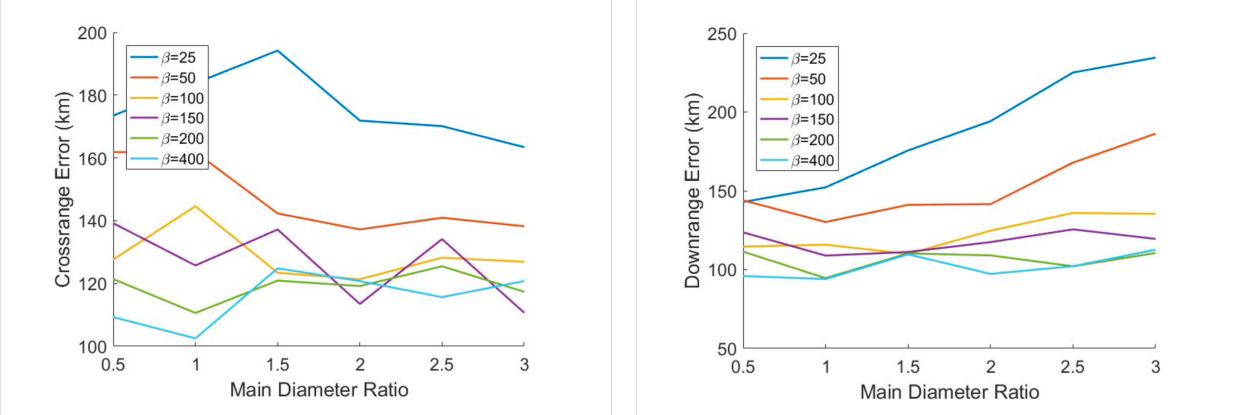

(a) Crossrange Error vs Diameter Ratio for 4 km/s entry velocity [64]

(b) Downrange Error vs Diameter Ratio for 4 km/s entry velocity [64]

Fig. 25 Landing crossrange and downrange errors for a 4 km/s entry velocity

Figure 26 shows the largest possible landing ellipse on Ligeia Mare. Even with a 20% increase this landing ellipse stays within the confines of the lake.

C. The Lander and Buoy

As discussed in Sec. IV.B.2, the design of the BOBII buoy was limited by a minimum bound of 4.5 m (from the length of the rocket), a maximum bound of 8 m (from the diameter of the aeroshell), and the need for thermal insulation. In addition to the physical bounds on the buoy, the buoy must be:

1) afloat,
2) stable,
3) thermally insulated from the surrounding liquid.

The first two requirements are straightforward. The delicate instrumentation inside the buoy must remain at the surface and be protected from tipping over. The last requirement is set to help achieve our science goals of analyzing liquid

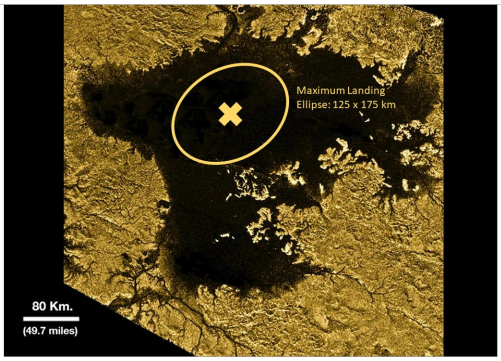

Fig. 26 Landing ellipse on Ligeria Mare

samples from Titan with minimal change to the sample compared to the environment it was taken from. Due to the nature of the methane lakes, even minor changes in temperature could significantly alter the composition of these liquids. At the same time, we must maintain near-room temperature conditions inside the buoy for the electronics. We therefore require thermal insulation between the outer shell of the buoy and the instrumentation inside to protect the lake from the thermal environment inside the buoy.

These requirements must be satisfied during two phases of operation: after landing and during the science operation. The first phase is with all the mass contained within the buoy, while the second phase is with the mass of the profiler assumed to no longer be exerting force on the buoy. To accomplish all three of these goals during both phases, we utilize a multi-material design for the buoy. A simplified cross-section of this design is shown in Fig. **??**. A table of components and their locations are listed in Table 9. The rocket, electronics, communication suite, and some instrumentation systems are kept in the top section of the buoy to keep them far from the liquid methane. The next layer is made of aerogel, a low-density, low-thermal conductivity material that isolates the lake from the heaters required to keep the electronics in the top section operational.

Within the base of the buoy, there are three main "shells" of materials. The innermost section is to store the profiler. Note that for structural analysis, this region has been approximated as a hemisphere; its actual structure more closely resembles a cylinder. The next layer out is constructed of G10, a fiberglass material with high density and relatively low thermal conductivity. This material can be outgassed before launch according to standardized procedures in order to prepare it for space conditions. The outermost layer is for ballast—as the buoy is very top-heavy due to the rocket and batteries contained in the top layer, we plan to fill the bottom with liquid methane through ports about the base of the buoy after arriving at Ligeia Mare as ballast to improve the stability of the buoy without requiring additional mass to be brought with us from Earth. Finally, the buoy is surrounded by a thin 316 stainless steel wall for its robustness and compatibility with cryogenic temperatures, although this component has been omitted for the purposes of the following analysis for simplicity.

Material	Density (kg/m^2)	Thermal capacity (W/mK)	Citation
Aerogel	20	0.02	[67]
G-10 fiberglass	1800	0.3	[68]
Stainless steel 316	7900	14.6	[69]

Table 9 Materials used in buoy design.

To determine the size of the buoy, we performed an analysis of multiple criteria addressing whether or not it satisfies the criteria set forth. In this model, we approximate the top two layers of rocket/instrumentation and aerogel as a discs of uniform density. The bottom half of the buoy is modeled as a series of hemispheric shells as seen in Fig. 13. We assume a height of 0.5 m for the aerogel layer, 1 m for the rocket/instrumentation layer (dictated by the diameter of the rocket), a diameter of 1 m for the profiler, and a diameter of 2 m for the insulating G10 layer. The variation of mass with changes in buoy diameter over a range of acceptable sizes is shown in Fig. 27a.

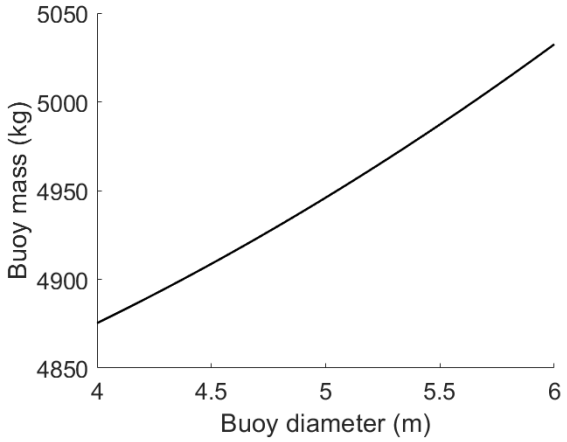

(a) Mass of the buoy with varying buoy diameter.

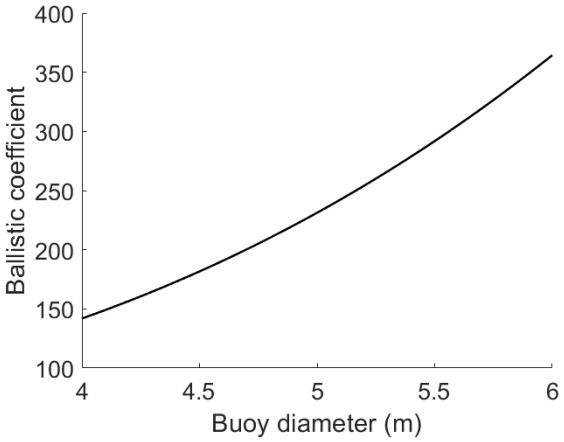

(b) Ballistic coefficient of buoy with varying buoy diameter.

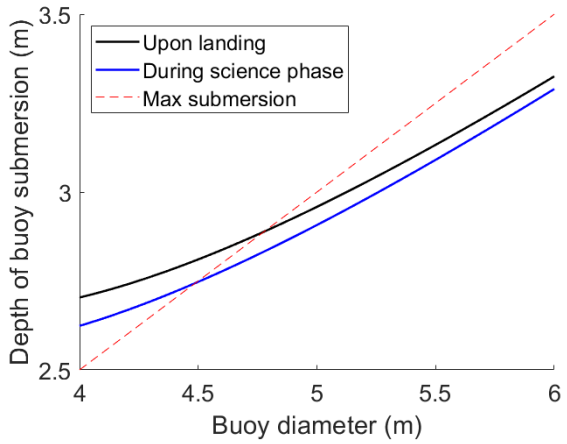

(c) Depth of buoy submersion with varying buoy diameter.

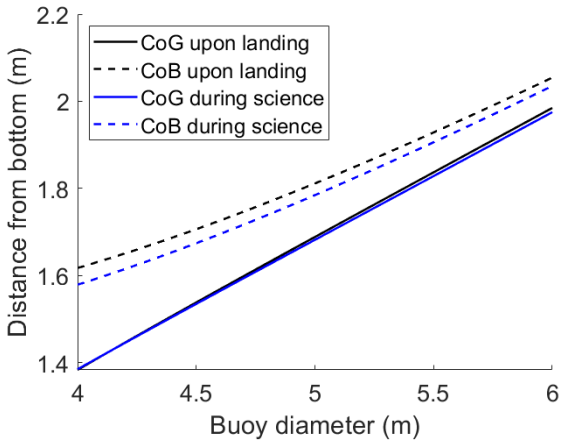

(d) Center of gravity and center of buoyancy with varying buoy diameter.

Fig. 27 Changes in various buoy parameters with diameter.

While the mass increases over this range of buoy diameters, the variation is less than 200 kg and all values fall into a reasonable range given our launch vehicle from Earth and mission timeline. All of them remain viable options for sizing the buoy. To analyze whether or not our first requirement that the buoy stay afloat is fulfilled, we determine the depth at which the buoy floats in the lake. To do so, we calculate the buoyancy force:

$$F_b = \rho_f V g, \tag{7}$$

where F_b is the buoyancy force, ρ_f is the density of the fluid, V is the volume of the fluid displaced, and g is gravity. The density of liquid methane at 91 K and 1.5 bar is 445.8 kg/m^3 and the gravity on Titan is 1.352 m/s^2 [70]. The buoy will float at a point at which the force of the weight is equivalent to the buoyancy force. We calculate the depth of buoy submersion that satisfies this condition by finding solving for the volume of displaced fluid given the weight of the entire system as seen in Fig. 27c.

The dashed red line indicates the maximum depth to which the buoy can submerge, which we define as the top of the aerogel layer such that we can maintain thermal isolation for the upper layer of the buoy. The buoy is more submerged upon landing than in it is during the science phase, with a minimum diameter of 4.8 m required for buoy to float sufficiently high in the water. We therefore have a minimum bound on our buoy diameter.

Finally, we check that the buoy is stable in the lake. For this condition to be satisfied, the center of buoyancy (CoB) must be higher than the center of gravity (CoG), where the center of buoyancy is defined as the center of gravity in the

volume of the fluid displaced by the body. The comparison of these locations is shown in Fig.27d.

Two caveats regarding our calculations of center of gravity and buoyancy are that firstly, we assume the mass of the WIF to be located in the center of the lower shell instead of the bottom, and secondly, we assume the mass of the rocket to be evenly distributed through the top layer. However, the more realistic cases in both these scenarios would only improve our stability as it would pull our center of gravity downwards without significantly affecting our center of buoyancy; our analysis therefore represents a conservative estimate. Over the entire range of buoy diameters, the center of buoyancy is located above the center of gravity for both the landing phase and the science phase. However, the distance between these two decreases with increasing diameter, indicating that the stability of the buoy decreases. It is therefore in our best interests to size the buoy as small as possible while maintaining the other conditions (flotation and thermal isolation). With these constraints in mind, we selected **5 m** as our radius for the buoy. This diameter allows our buoy to float at an acceptable depth in the lake and minimize its weight while maintaining its stability.

The buoy must satisfy one other requirement during its tenure. For the ascent phase, the rocket will be launching off of the buoy and using it as a launchpad. While thermal isolation will no longer need to be maintained during this phase as the samples will have already been collected, we do still need to maintain the buoy's flotation and stability. In the worst case scenario, the buoy is fully submerged. In this situation it would exert a buoyancy force of over 30 kN for the 5 m diameter buoy, which is more than an order of magnitude higher than the thrust of 2000 N being exerted on the float. We therefore expect that we are able to launch the ascent vehicle without issue.

1. Buoy Subsystems

Thermal Given the harsh cold temperatures of the dense Titan atmosphere and lakes, many thermal considerations must be made to ensure the spacecraft, lander, and ascent vehicles maintain the operating temperatures of all of the components on-board. Most restrictive are the many electrical components that require warmth to operate optimally, such as the battery and any electrically powered mechanisms. Several forms of active and passive thermal control must be used on all aspects of the mission to ensure that the heat generated will be maintained.

The average temperature of the lake surface, where the main buoy and electronics sit, will be around $93.65 +/- 0.15$ K. The profiler may be subjected to colder temperatures as it descends the lake. Due the thick atmosphere and low solar flux, Titan exhibits little diurnal temperature variations on the surface [71].

Given the extreme temperatures of Titan, active thermal controls will most likely be needed, rather than relying on passive heat generation from electronics. The main methods of active thermal control considered were electric heaters, liquid and pipe cooling/heating systems with an RTG, thermal batteries, and Radioisotope Heating Units (RHU). A simple high level comparison was made to evaluate these options.

Given the power efficiency and simplicity of the RHUs, these individual discrete units can easily be distributed throughout the spacecraft along with passive thermal insulation materials to retain heat. The radiation generated will be shielded by existing radiation protection casings for electronics, with additional as needed. If additional heating is necessary, thermal batteries may be considered, with the trade of less energy-density from a power standpoint, and in turn, more mass.

Power The Titan surface provides a challenging location to design a sustainable power system. Due to the low solar flux and extremely cold temperatures, the power system must be considered carefully. A high-level assessment was made of the following technologies: RTGs, Lithium Ion Batteries, Solar Panels, and Thermal Batteries.

The low solar flux on Titan make solar panels as an extremely cost and mass-ineffective solution. Solar panels would need to be 400x the size as earth-orbiting satellites, and performance decreases with the constant haze [71]. Given the high-risk and thermally challenging case of an RTG as mentioned in the previous section, single-use batteries are much more attractive. Since the buoy is subject to mass constraints, the energy-dense lithium ion batteries are the most feasible option. Numerous batteries have flown in proven environments, and the battery design can be modeled off of GPM's power design [72]. As mentioned before, if additional heating is needed, thermal batteries may be considered. Since the lander will not be in contact with the Earth once the orbiter leaves, the payload will not need to continue science.

In order to sustain all of the sample collection operations, the power draw was calculated for each operating mode of the nominal mission lifetime. These modes were derived from splitting up the surface operations CONOPS, and the time spent in each operating mode is then derived. Science instrumentation operation, communications, sample

	Component	Max Power (W)	on/off	Profiler Traversal	on/off	LIBS/Raman Confirmation	on/off	Comms	on/off	Sea-Floor Mapping	on/off	Idle
Profiler/Sampling	Motor/Spool	60	1	60	0	0	0	0	0	0	0	0
	Proximity Sensor	0.5	1	0.5	0	0	0	0	0	0	0	0
	Core Drill	20	0	0	0	0	0	0	0	0	0	0
	Misc.	5	0	0	0	0	0	0	0	0	0	0
Instrumentation	LIBS-Raman #1	70	0	0	1	70	0	0	0	0	0	0
	GC-MS	100	0	0	0	0	0	0	0	0	0	0
	Titancam-Z	40	0	0	0	0	0	0	0	0	0	0
Collection Context	Pressure/Temperature/Turbidity	2	1	2	0	0	0	0	0	0	0	0
	IR Lightbulb	5	0	0	1	5	0	0	0	0	0	0
	Sidescan SONAR	25	0	0	0	0	0	0	1	25	0	
	Depth Sounder	2	0	0	0	0	0	0	1	2	0	
Communications	S-Band Transmitter	50	0	0	0	0	1	50	0	0	0	0
	X-Band Transmitter	50	0	0	0	0	0	0	0	0	0	0
Thermal	Cryogenic Cooling Pump	5	1	5	1	5	0	0	0	0	0	0
	RHU	0	1	0	1	0	1	0	0	0	0	0
Misc	On-Board Computer	10	1	10	1	10	1	10	1	10	1	10
				0		0		0		0		0
	Watts	444.5		**77.5**		**90**		**60**		**37**		**10**
	Total Time Spent in Mode (Hrs)			77		10		100		5		960~

Table 10 Power budget overview.

collection, and idle modes are considered. For all instrumentation, values were pulled from previous missions with similar instrumentation systems, primarily the Mars Rover missions.

Power analysis over the course of the mission is done by iterating the power draw over different load profiles to determine the approximate capacity, and ultimately, the density necessary to support a nominal mission life-time of about 1.5 months for all science operations. The analysis was performed for a Sony 18650 HC battery with the corresponding discharge curves[73]. The graph below showcases the total battery discharge expected after being subjected to the expected loads for their respective amounts of time.

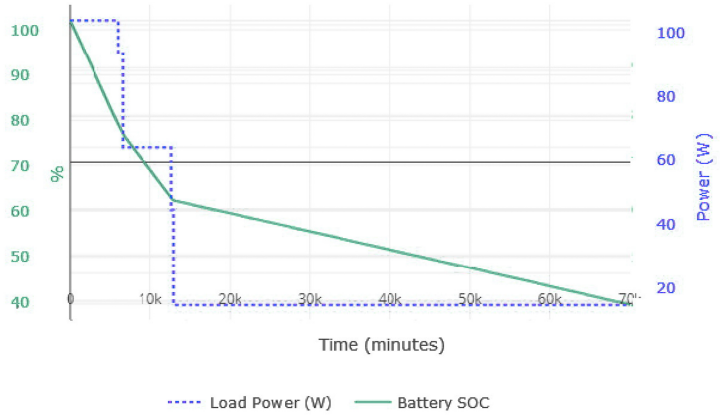

Fig. 28 Battery total discharge and load profile representing aggregate time for different operating modes for 50 days

A capacity of 1380 Ahr was found to be necessary for the duration of the mission. At the end of 70,000 minutes (almost 50 days), the remaining battery state of charge (SOC) is around 40%. This large margin provides additional time for troubleshooting, additional science, entry, and ascent. Given the energy density of the cells, an approximately 300 kg mass would be needed to sustain all operations [74]. The mass can be split up into approximately six discrete 50 kg cells spread out throughout the buoy.

D. Titan Ascent Vehicle

Successfully storing, launching and rendezvous-ing with the orbiter presents a single-point-of failure system design issue for returning all collected atmosphere and lake samples to Earth for further evaluation. Several high-level designs including a high altitude ballon, multi-stage rocket, and drone were considered for ascent from the surface. Once a rocket was determined to be most feasible, several configurations for sea launch were compared [40, 75]. Taking into account unique challenges of thermal insulation, long term storage and operation of a launch vehicle, lack of knowledge about Titan surface weather, and round-trip delayed communication of more than two hours, the proposed Titan Ascent Vehicle (TAV) is a single-stage to orbit gimballed liquid rocket which would have substantial thermal insulation, minimal complexity of mechanisms, and redundant systems. Preliminary study into an ascent trajectory from Titan indicate that a LOX/LCH4 engine with 290 s specific impulse and 1.5 kN of thrust may be a viable configuration for launch due to long-term effort for qualification and storage of these propellants as well as potential for ISRU [41, 76]. The vehicle would have an approximate mass of 658kg, diameter of 0.5m and height of 4.5m. It would contain a hermetically sealed and insulated sample container and launch from the surface from the vertical configuration using a pneumatic toss like the MAV [40].

Trajectory Design The target orbit is 1500 km circular orbit, with a ΔV of 4.0647 km s^{-1}. The altitude of Ligeia Mare is approximately 600 m below the surface of Titan. A simple density model was extrapolated from HASI and Cassini data to calculate the density up to 1150 km, above which the effects of drag from Titan's oblateness are greater than the effects of the drag, so drag was neglected above this altitude [77, 78]. This resulted in a trajectory with a 20 minute burn followed by 11 minutes of coasting where the rocket accelerates to greater than 1460 km s^{-1} by the altitude of 1500 km. Final circularization may be done with an extra 5 kg of propellant mass, cold gas thrusters, or a reaction wheel allowing for an additional 50m s^{-1} ΔV. The sample container contains no navigational ability and would be brightly colored for visual retrieval once ejected into the appropriate orbit.

In a theoretical study intended to return eight times the sample of this mission, the system for a 4000 kg rocket was a two stage methane/LOX rocket with a first stage optimized to 270 s and a second stage optimized to 310 s [41]. The maximum theoretical specific impulse of this propellant is 345 s [79]. This study assumes a specific impulse of 290 s and models of a two stage and single stage engine were analyzed along with a variety of design thrusts and firing times to optimize for hitting 1500 km at close to 1480 km s^{-1}.

Vehicle Design The rocket was designed backwards from the required thrust for an 18kg payload with a 0.85 structural coefficient (ϵ) limit in mind. The TAV has a 90 kg structure and 595 kg of propellant, with a 2.55 oxidizer to fuel mass ratio. There are two propellant tanks, a metal bladder for cryogenic blowdown, and mechanisms for gimballing the engine and ejecting the sample container. Dual sample insertion ports, a backup release mechanism for ejection, and cold gas thrusters for final control provide redundancy on ascent. Estimates show the structure and the payload must withstand a max load of 1.2g's seen in Fig. 29c. Titan's low gravity and high drag place importance on minimizing drag coefficient, but may allow for innovation in horizontal wings for lift. Future advances in launch vehicle technology would refine the vehicle design to better leverage the unique properties of Titan's atmosphere.

Since the rocket is stowed horizontally, both rotating the rocket for launch and tossing the rocket horizontally were considered [40, 75]. The former involves complexity of mechanisms on the buoy and stability and thermal issues on the surface of the buoy and the lake, while the latter involves mechanism complexity, timing issues, and control during the rocket ascent. As the exhaust was calculated at 1344 K for this propellant system [41, 80], a pneumatic toss in vertical configuration was baselined. In the worst case the buoy could withstand the force of launch and a thermal blanket may protect the surface. However, the horizontal configuration would be more appealing for future analysis and minimize both the mass of rotation mechanisms and risk to the lake environment if it proves successful in Mars sample return.

Avionics Design A reliable attitude determination and control system (ADCS) and avionics design is crucial to the success of the TAV. The avionics must be as light and robust as possible, which informed design cues from the MAV designed for the Mars Sample Return Mission [40]. The TAV avionics are responsible for telecommunications with the orbiter, command and data handling, and power distribution. Avionics hardware includes a power distribution board, ADCS system, pyro controller board, flight computer, thermal batteries, inertial measurement unit (IMU), transmitter, and antenna. Communications with the orbiter are handled over a 2.4 Ghz signal transmitted through the antenna. The functional requirements of the TAV avionics section are met by the NASA Sphinx flight computer, a custom ADCS board and pyro controller, and a miniature IMU of the same scale and performance as the Honeywell MIMU selected for the MAV [40].

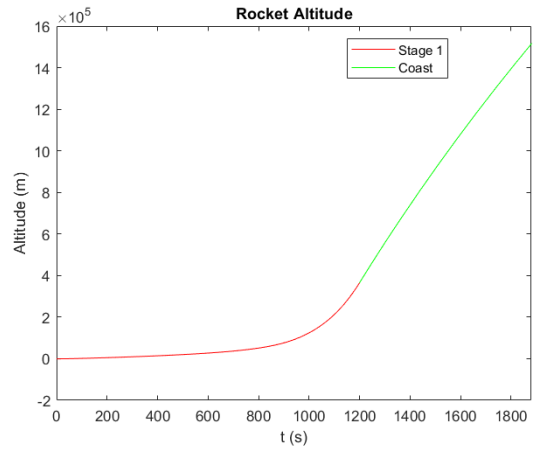

(a) TAV Altitude with 20 minute burn at 1.2 kN

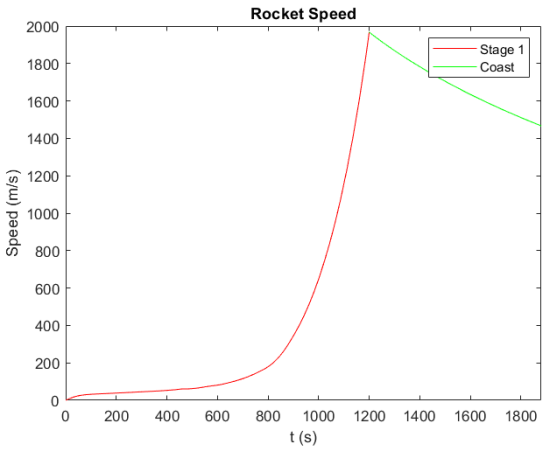

(b) TAV Velocity with 20 minute burn at 1.2 kN

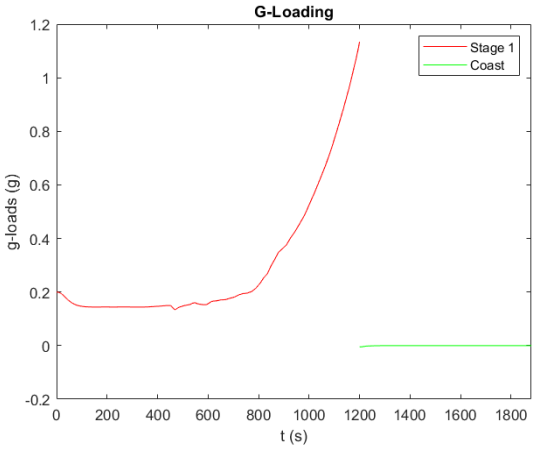

(c) TAV Acceleration with 20 minute burn at 1.2 kN

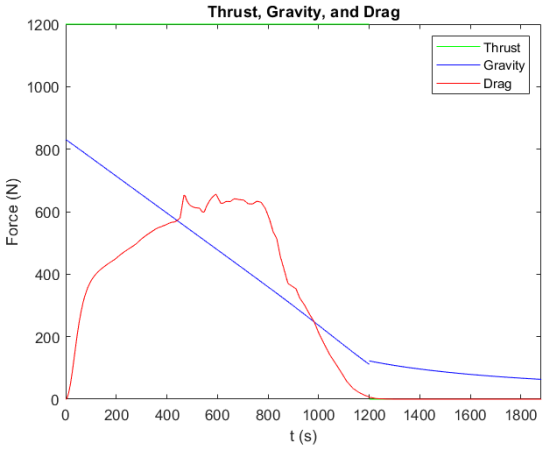

(d) TAV forces with 20 minute burn at 1.2 kN

Fig. 29 Engine performance model for a simplified Titan Ascent Vehicle

The TAV RCS provides attitude control through the actuated stabilizing fins and the nozzle gimballing of the TAV rocket motor. The actuated stabilizing fins provide roll stability through an optimally derived guidance control law during the rocket's powered ascent, and the nozzle gimballing allows for maintaining trajectory and stabilizing during launch.

Thermal Considerations Thermal batteries provide power to the entire RCS after launch. These batteries are single use, so the pre-launch systems are integrated with the buoy until launch is initiated, and the thermal batteries provide power to the pyro controller board and ignite the rocket. The thermal batteries chosen for the TAV are four Eaglepicher EAP - 12326 batteries pulsing 21A, with the first two squibbed at launch and the next two squibbed as the first set runs out of power. Thermal batteries are flight proven technologies used in a variety of guided rockets, including the MAV [40]. The avionics are powered by a 3500 mah battery that provides 10A of power to the avionics section, a figure derived from the similar power requirements for the MAV DAC 0.0 [40]. This battery is kept at optimal operating performance throughout the duration of the mission.

The TAV is exposed to cryogenic temperatures of 91K at the surface of Ligea Mare that will inhibit the performance of crucial avionics unless kept at a temperature of 300 K. The TAV is stored flush with the top surface of the buoy, and the avionics and thermal batteries are kept insulated within a MLI shell surrounding the nosecone and avionics section of the TAV while being heated by the thermal management systems that keep sensitive instruments on the Buoy at operating temperatures.

The engine of the rocket can be cooled using typical film cooling techniques. The tanks will remain slightly above 90 K

through insulation and slight contact with the MLI shell. During the trip to Titan, there will need to be some active cooling of the cryogenic pressurized tanks as well as insulation from the control avionics and sample compartment.

E. Rendezvous, Retrieval, and Return

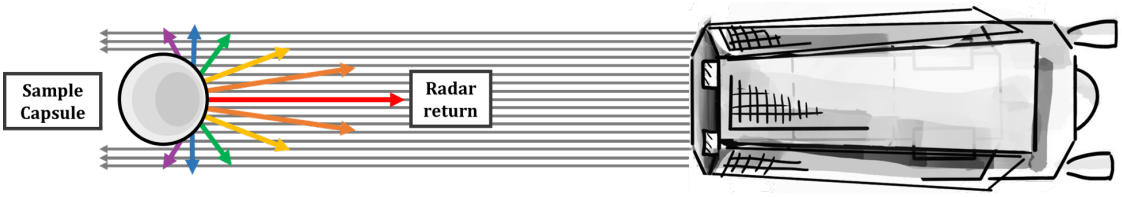

Fig. 30 Notional diagram illustrating the radar return of a spherical bare-metal sample capsule.

The rendezvous phase is broken down into three stages. First, target identification addresses how the target pixels get resolved and identified against the optical environment in an image. Second, relative state estimation addresses knowledge of the relative orbits between the target and chaser. Third, relative control applies the desired ΔV towards rendezvous. The proposed geometry of the sample capsule is a bare metal sphere for two reasons. First, the radar cross section (RCS) of bare metal is most reflective to the radar sensor, and a sphere makes the radar return orientation-agnostic. Figure 30 illustrates a sphere's isotropic reflection as a projected circle to the receiver. Second, a spherical geometry means that the physical mechanism of capture need not worry about the attitude and angular velocity of the sphere in-orbit. Thus, there is no need for attitude synchronization in order to fit the capsule shape into the capture port.

1. Target Identification

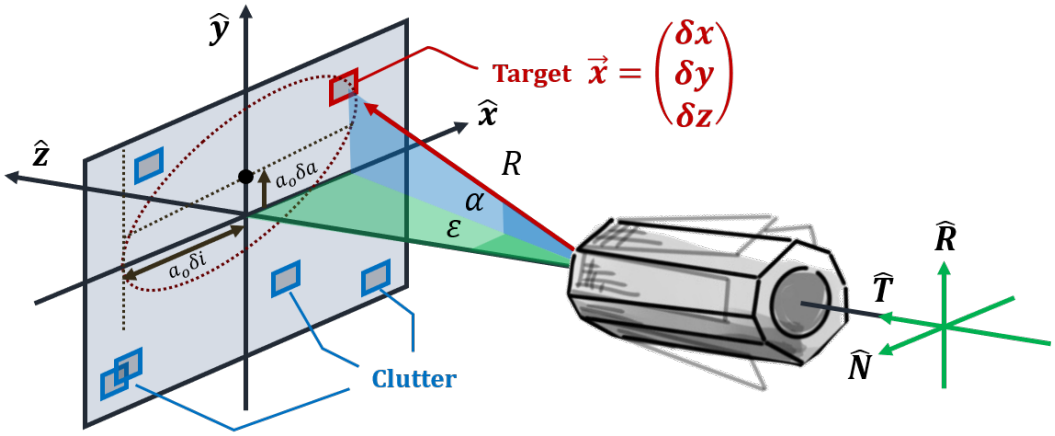

Fig. 31 Projected target's relative orbit geometry, amidst clutter, in the vision-based sensor's frame

The first challenge in the rendezvous phase would be to distinguish the actual target among potential clutter in radar returns at far-range, and against the visual backdrop of stars at visual range. The lack of space heritage in deep-space target identification poses a key technical gap and risk. The present state of the art that addresses this challenge will be validated in the upcoming NASA Starling Mission [81]. First, in order to distinguish luminous stellar objects from the target, legacy algorithms such as PYRAMID can be employed [82]. Next, to distinguish non-stellar objects from the target, the relative orbital dynamics can be exploited to distinguish the target from clutter during target tracking. To do so, the target's state representation is important. For proximity ops, the target relative state is best represented by a set of quasi-nonsingular relative orbital elements (ROE) as formulated by D'Amico [83]. In this formulation, a geometrically intuitive linear map exists between the target ROE and its non-dimensional relative position in radial-transverse-normal (RTN) frame. A notional mapping on the RN-plane is shown in Figure 31. This geometry is exploited in Starling using a multi-hypothesis tracking algorithm, SAMUS [84] which collects angular measurement data about one or more

potential targets, maintains a set of tracks produced by each target over time, and selects the most likely hypothesis. The dynamics are exploited where the most likely target would have a projected relative motion (as seen by the vision-based sensor) that reasonably obeys the geometry interpreted by the ROE states. Demonstrator missions such as Starling will be critical intermediaries that narrow the technical gap for target identification in our proposed mission.

2. Relative Navigation

Once the target is identified, the chaser (orbiter) exploits local azimuth, elevation and range measurements to perform relative state estimation of the target (sample capsule), using a sensor suite comprising of a radar sensor and an optical camera. This is a standard suite for targeting missions, such as Hayabusa-2's rendezvous with Ryugu as an example [85]. The key requirement is centimeter level relative navigation between chaser and target during physical capture at close range. This has to be done autonomously due to the time-critical nature of rendezvous which cannot afford signal delays with humans-in-the-loop between Earth and Titan. Thus, a sequential filter is necessitated. However, high-precision relative navigation in deep space is an untested challenge. This is compounded by limited gravimetric data about Titan. Thus, orbit propagation in the navigation filter may rely at best on the degree 2 hydrostatic terms and the sectorial harmonics of degree 3 [62]. A generalized Kalman-filtering framework for a navigation filter with target identification is presented below in Figure 32,

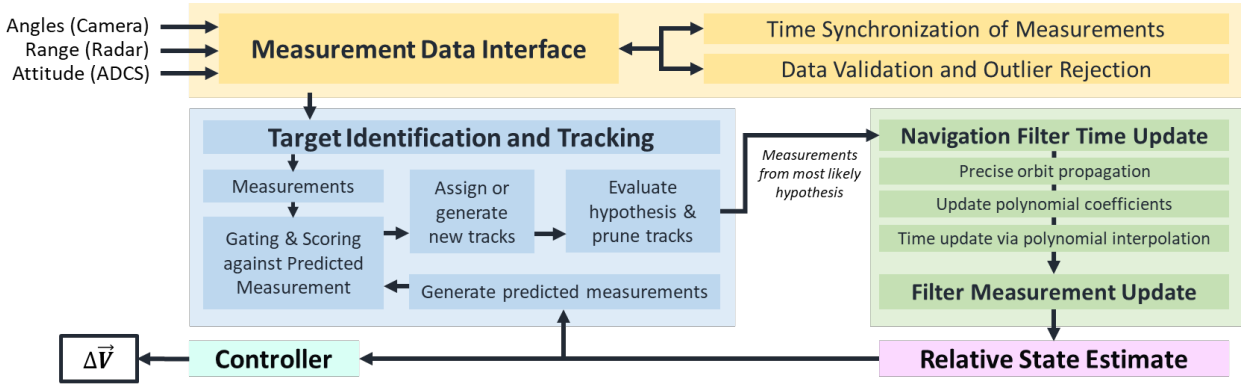

Fig. 32 A generalized navigation filter with target identification during sample rendezvous

The filter architecture begins with interfacing with measurement data for basic validation, outlier rejection, and time-tagging. Coordinate transformations between body-frame and sensor-frame are also continually maintained. The navigation time-update performs a precise orbit propagation accounting for higher-order geopotentials of Titan [62], atmospheric drag, and Saturn's third-body effects. The propagated states are used to construct or update a quintic Hermite polynomial fitted to the relative state estimates. The polynomial allows for on-demand interpolation of state estimates at finer time-resolutions without costly orbit propagations. Such a framework had been successfully implemented in the PRISMA mission [83]. The measurement update uses the model in Eq 8, referenced to the vision-based sensor frame in Figure 31. The measurement model is

$$\vec{h} = \begin{pmatrix} \alpha \\ \varepsilon \\ R \end{pmatrix} = \begin{pmatrix} \arcsin\left(\delta y \;/\; \|\vec{x}\|\right) \\ \arctan\left(\delta x \;/\; \delta z\right) \\ \|\vec{x}\| \end{pmatrix} \tag{8}$$

To narrow the mission risks further, it is proposed that (i) a prior demonstrator mission for rendezvous be rigorously tested in Earth orbit using the same radar and optical sensors proposed, and (ii) a further collection of gravimetric and atmospheric density data about Titan is needed to increase the fidelity of the orbit propagator's knowledge of Titan's geopotentials and drag forces in the navigation filter. This will aid in passing accurate and reliable state estimates to the controller, not only during filter time updates, but also in the event of a measurement black-out.

3. Relative Control

Model predictive control (MPC) is the candidate form of control explored in this study due to its ability to minimize multiple performance costs critical to the safe rendezvous of the samples. These costs are predicted over finite horizon based on the relative dynamics between the orbiter and sample capsule. Specifically for this mission, the controller penalizes (i) the relative state difference between the orbiter and samples, (ii) the control effort or ΔV usage for rendezvous, (iii) a terminal relative state cost so as to maximally achieve a "soft" impact rendezvous, in hopes of preventing collisional damage to the samples. The quadratic objective function is modelled in Eq 9,

$$J(\delta\vec{x}_k, \vec{u}_k) = \sum_{\ell=0}^{M-1} \left[\underbrace{\|\delta\vec{x}_{k+\ell}\|_P^2}_{\substack{\text{penalty on} \\ \text{state error}}} + \underbrace{\|\vec{u}_{k+\ell}\|_Q^2}_{\substack{\text{penalty on} \\ \text{control effort}}} \right] + \underbrace{\|\delta\vec{x}_{k+M}\|_R^2}_{\substack{\text{terminal relative} \\ \text{state cost}}} \tag{9}$$

where the variable k is the first epoch in the receding horizon on the absolute time scale, ℓ is the current time step within the receding horizon, $\delta\vec{x}$ is a relative state between the orbiter and sample capsule, using some general state representation (position-velocity or orbital elements), $\vec{u}$ is the controller output ΔV, index M is the maximum horizon of the prediction window, matrices P, Q, R, S are the positive definite matrices defining penalty weights in the Mahalanobis norms. The inclusion of penalty methods also converts a constrained optimization problem to an unconstrained one. The resultant controller's output $\vec{u}$ can then be obtained by repeatedly minimizing Eq 9 online.

If the relative dynamics can be linearized and discretized in the form 10 using a suitable state transition matrix **A** with a controller input mapping **B**, and assuming that the linearization remains constant over the receding horizon, then

$$\delta\vec{x}_{k+1} = \mathbf{A}_k\delta\vec{x}_k + \mathbf{B}_k\vec{u}_k \tag{10}$$

In this form, an analytical closed-form solution that approximates the optimal control effort exists, as the linearized dynamics allows for closed-form prediction of future states simply by cascading the transition matrix **A** at epoch k by the number of time steps. This makes the controller extremely efficient computationally. By taking the derivative of Eq 9, setting it to zero, we arrive at a closed-form control solution $\vec{u}_{k+\ell}$,

$$\vec{u}_{k+\ell} = -\mathbf{Q}^{-1}\mathbf{B}_{k+\ell}^T \left[\mathbf{P}\delta\vec{x}_{k+\ell+1} + \left(\mathbf{A}_{k+\ell}^T\right)^{M-1} \mathbf{R}\delta\vec{x}_{k+M} \right] \tag{11}$$

Validating this control law, we simulated a scenario where the sample capsules were injected into low Titan orbit with semi-major axis error $\Delta a = -25km$ lower than expected and with a $\Delta i = 1^\circ$ orbit plane error from the orbiter. The relative state vector terms in $\delta\vec{x}$ are the first order differences of a Taylor expansion taken about the quasi non-singular orbital elements $[a, e_x, e_y, i, \Omega, u]$ of the orbiter (in other words, they are first order differences between the orbiter and sample orbit elements). The requirement of precise (cm-level) relative state knowledge was assumed satisfied. The prediction horizon was set to be $M = 12$, with total ΔV bounds per horizon capped at ±5 m/s. Matrices **P, Q, R, S** were manually tuned. Figure 33a illustrates the orbiter's trajectory in the RTN frame, while Fig. 33b indicates convergence not only in relative position, but also gradual convergence in relative velocity which is necessary for a "soft" impact rendezvous. **The total ΔV required for the rendezvous operation was 46.837m/s.**

F. The Communication Systems

The sample collection mission involves a spacecraft which consists of an orbiter plus lander system. Once the lander is deployed, the orbiter revolves in a circular orbit around Titan at an altitude of 1500kms. This section explains the telecom design for the complete mission divided into the following parts -

1. Telecom System requirements

The Earth is considered as a point source when evaluating distance for link budgets from Orbiter or lander. Also, the distance from orbiter to the Earth, or lander to the Earth is considered the same for ease of calculations. Atmospheric models for attenuation to RF frequencies in Titan's atmosphere were unavailable during the time of this study. So

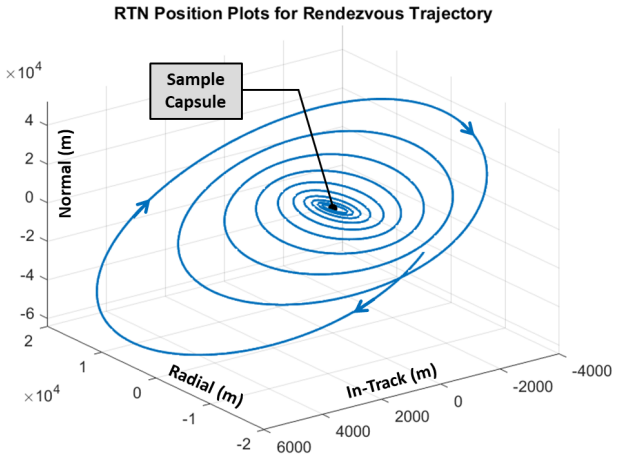

(a) Relative position plot in 3D RTN frame

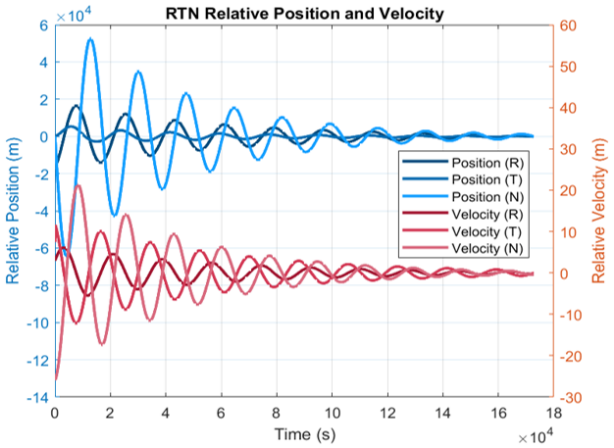

(b) Relative position in RTN against time

an additional 2dB path loss is factored in to represent all attenuations while calculating the link budgets. The target bit error rate (BER) is assumed to be 10^{-8}. The uplink data rate requirement is assumed to be 500 b/s. However, it is shown later that higher data rates are achievable by appropriately increasing the DSN transmitter power. All link budgets are plotted for the worst case scenario which assumes maximum distance between the Earth and Orbiter, which is $9.28 * 10^{11}$ meters. The science mission includes a variety of payloads that generate a lot of data. The bottleneck in this system design is transmission of the data back to the earth. Maximum possible area and power was allocated to the high gain orbiter antenna to send the data back to the earth.

2. High-level system design and trade-off study

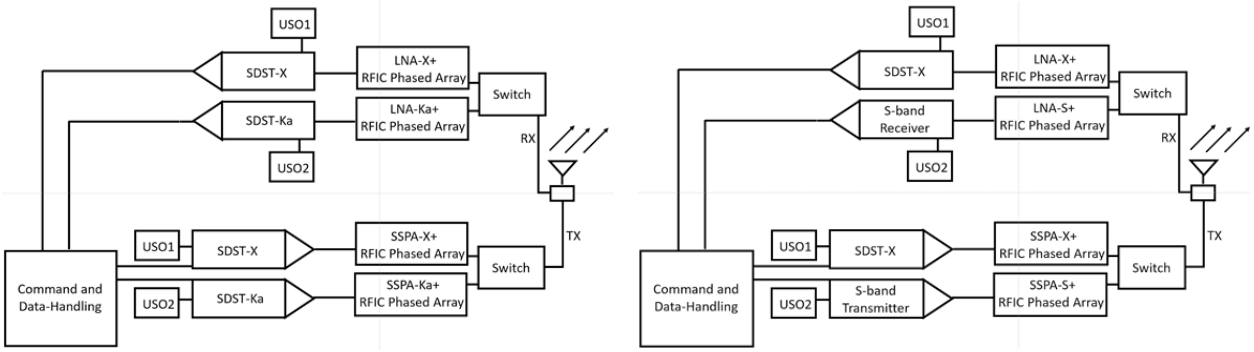

(a) **(b)**

Fig. 34 High level block diagram for the telecom system. (a) HGA (X+Ka band) on Orbiter (b) LGA (S+X band) on orbiter and lander.

Fig. 34 shows the high level block diagram of the communication system. This telecom system design exclusively uses phased array antennas for both the orbiter and landers. The orbiter uses a dual resonant high gain antenna (HGA) operating in the Ka-band and X-band, with right-hand circular polarization (RHCP) polarization. It also has a dual resonant low gain antenna (LGA) operating in the X-band and S-band, also with RHCP polarization. The same dual-band RHCP LGA is also present on the lander. The above figures show the block diagram of the communication system for the HGA and LGA respectively. It is seen that the block diagrams consist of a small deep space transponder (SDST) [86] that is developed for the X-band and K-band by Jet Propulsion Laboratory. An earlier version of the same transponder was used for the Cassini-Huygens mission [1]. The same transponder is also used in the Mars reconnaissance orbiter mission [87], the Juno mission [88] and the proposed Titan Explorer mission [87]. All of those missions however, used a traveling wave tube amplifier (TWTA) for the power amplifier in the transmitting path. The TWTAs however, are susceptible to failure over long mission durations [89]. An alternative solution is use of solid-state power amplifiers

(SSPAs) that can serve as a replacement to TWTAs [90],[91]. The SSPAs are a proven technology with the European space agency (ESA) showing a TRL6 level 100W-Ka band SSPA implementation [92], and the use of lower rated SSPAs in the Marco-A and B missions [93]. Fig. 35 below shows a trade-study between SSPAs and TWTAs that lists the pros and cons for both technologies. The ultra stable oscillators (USOs) are cross-strapped (cross-strapping not shown) so that, if one fails, the other can be used by either SDST.

Sr. No	SSPA	TWTA
	Pros	***Pros***
1	Less Space and Weight Requirement	More proven technology backed by multiple mission implementations
2	More reliable GaN solid-state technology with longer operating life	Generally higher drain efficiencies as compared to SSPAs
3	Low leakage voltage due to gate insulation in the OFF State	

Fig. 35 High level trade study SSPA vs. TWTA

In recent times, the evolution of phased arrays as a technology has enabled possibilities for precise electronic beam steering at very fast speeds, which was non-realizable more than a couple of decades ago [48]. Phased array antennas have a lot of advantages over the dish antennas. The salient features of both technologies are compared in the Fig. 36.

Sr. No	Phased Array Antennas	Dish Antennas
	Pros	***Pros***
1	Considerably less antenna weight.	Can have higher bandwidths than phased arrays.
2	Better space optimization due to planar structure	Can act as heat or debris shields for rest of the sub-systems
3	Considerable fuel saving by reducing spacecraft maneuvers.	Greater mechanical strength and durability.
4	Marginal power saving by elimination of antenna rotating gimbals.	Need less active circuits than phased array antennas (Phase shifter RFIC eliminated)

Fig. 36 Phased arrays and dish antennas trade study

Fig. 37 below show the general design of a phased array antenna based on stacked patch elements along with element sizes and their spacing. The feeding network and phase shifter RFIC is not shown in this figure. The design concept is similar to the implemented dual-polarized phased array antenna system shown in [93] having 55dB gain.

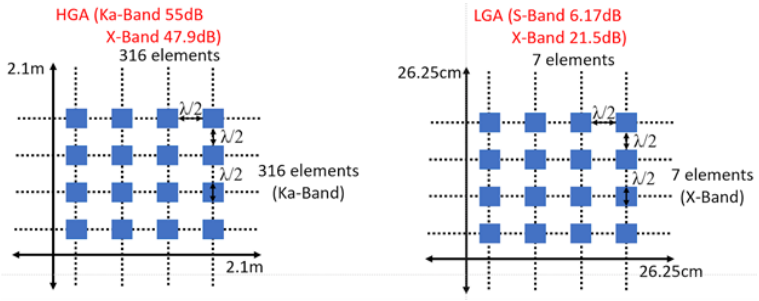

Fig. 37 Stacked patch antenna conceptual design for dual-band operation. (a) Antenna that resonates in Ka-band and X-band with indicated gains (Only bottom Ka-Band layer shown). (b) Antenna that resonates in S-band and X-band with indicated gains (Only bottom X-Band layer shown).

To achieve the BER of 10^{-8} mentioned earlier, various modulation schemes were tried with different modulation indices in an additive white gaussian noise (AWGN) channel. Different modulation schemes have different BER probabilities, with certain schemes requiring less C/N0 ratios to achieve the 10^{-8} BER values. Figure. 38 shows the plots for BER vs C/N0 for different modulation schemes. QPSK, MSK and FSK perform similarly for the simulated channel and modulation index value of M=4. The C/N0 of 12dB results in a BER of 10-8 thereby allowing for superior data rates. Hence QPSK was selected as the encoding and decoding scheme for all data transmitted and received. The nominal operational flowchart for the communication systems is shown in Fig. 38

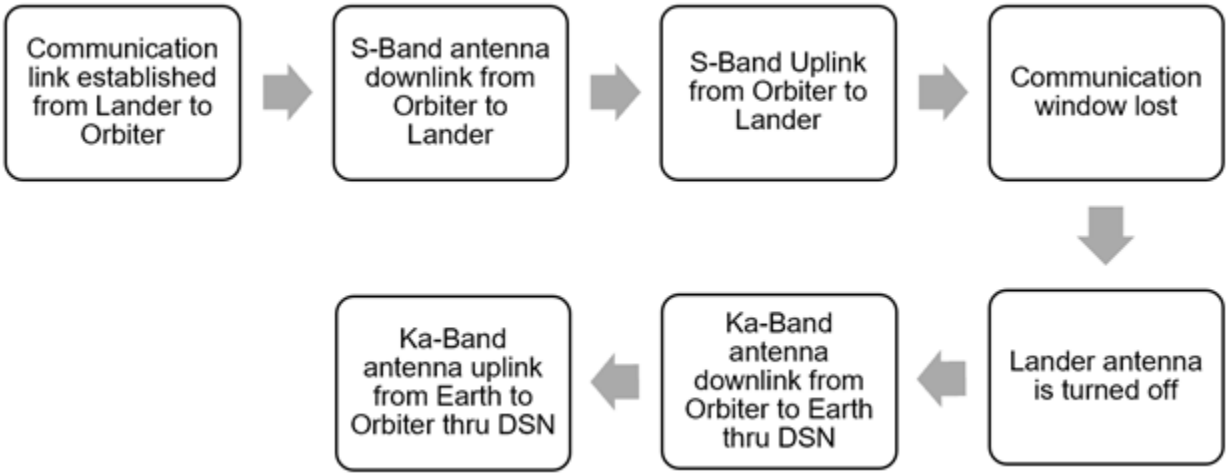

Fig. 38 Telecom operations flow chart

Figure 39 shows how the telecom window varies with respect to each orbiter passage. This indicates that the average window is about 40 mins at each pass with there being 2.5 passes in 24 hrs.

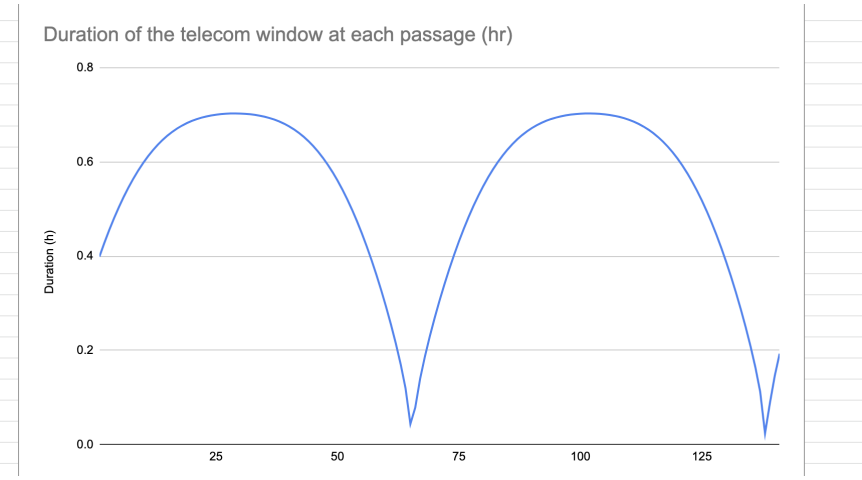

Fig. 39 Duration of the window per passage

Fig. 40 displays the different uplink and downlink scenarios possible for the telecom system consisting of Earth, orbiter and the lander. The three nominal cases are highlighted in yellow and all the rest of the scenarios are redundancy scenarios, in case one or multiple sub-systems fail. Thus the designed telecom system is a multiple-fault tolerant system that works even if more than one sub-systems fail at a given time.

Downlink	Use case
S-band Lander (LGA) to S-band Orbiter (LGA)	Emergency. Only if X-band antenna on Lander or Orbiter (both LGA and HGA) fails
X-band Lander (LGA) to X-band Orbiter (LGA)	Nominal Case
X-band Lander (LGA) to X-band Orbiter (HGA)	Extremely high data rate, but tracking very difficult
S-band Orbiter (LGA) to S-band DSN (70m)	Emergency. Only if Oriter Ka-band (HGA) and X-band (LGA and HGA) fail
X-band Orbiter (LGA) to X-Band DSN (70m)	Emergency. Only if Oriter Ka-band (HGA) and X-band (HGA) fail
S-band Lander (LGA) to S-band DSN (70m)	Emergency. Only if all Orbiter antennas and Lander X-Band (LGA) fail
X-band Lander (LGA) to X-Band DSN (70m)	Emergency. Only if all Orbiter antennas fail
X-band Orbiter (HGA) to X-Band DSN (70m)	Nominal Case
X-band Orbiter (HGA) to X-Band DSN (34m)	Only if Oriter Ka-band (HGA) fails
Ka-band Orbiter (HGA) to Ka-Band DSN (34m)	If X-band (70m) DSN is down
Uplink	**Use case**
S-band Lander (LGA) from S-band Orbiter (LGA)	Emergency. Only if X-band antenna on Lander or Orbiter (both LGA and HGA) fails
X-band Lander (LGA) from X-band Orbiter (LGA)	Nominal Case
X-band Lander (LGA) from X-band Orbiter (HGA)	Extremely high data rate, but tracking very difficult
S-band Orbiter (LGA) from S-band DSN (70m)	Emergency. Only if Oriter Ka-band (HGA) and X-band (LGA and HGA) fail
X-band Orbiter (LGA) from X-Band DSN (70m)	Emergency. Only if Oriter Ka-band (HGA) and X-band (HGA) fail
S-band Lander (LGA) from S-band DSN (70m)	Emergency. Only if all Orbiter antennas and Lander X-Band (LGA) fail
X-band Lander (LGA) from X-Band DSN (70m)	Only if all Orbiter antennas fail
X-band Orbiter (HGA) from X-Band DSN (70m)	Nominal Case
X-band Orbiter (HGA) from X-Band DSN (34m)	Only if Oriter Ka-band (HGA) fails
Ka-band Orbiter (HGA) from Ka-Band DSN (34m)	If X-band (70m) DSN is down

Fig. 40 Downlink and Uplink nominal and redundant cases

VI. Conclusion

Titan is a fascinating satellite with many mysteries we have yet to uncover. It has many geological processes that are similar to those we see on earth, yet foreign due to the materials present. Additionally, this Saturnian moon is a major talking point within the astrobiology community, as it has potential to harbor life as we do not know it within its organic-rich lakes. This mission aims to address questions concerning Titan's lake habitability and possibility for extinct or extant life by collecting, analyzing, and returning samples from the atmosphere directly above the lakes, the liquid within the lakes, and the solid material on the lake beds. Once returned to Earth, scientists will have the opportunity to conduct further experiments on the samples to reveal further clues that may lead to answering the question of Titan's potential to harbor life. Regardless of the outcome concerning life, this mission could address other research areas such as co-crystal formation, the replenishment source of methane, the origin of the light carbon ratio, the phases found within the lakes, whether the lakes are part of a kasrtic system, and many more fascinating questions. It would also provide much needed information of the vertical temperature, pressure, and compositional profiles of Ligeia Mare as well as the porosity of the lake beds, the size of waves, and the wind speeds and sub-lake surface currents. The TURTLE mission concept presented in this paper represents a novelty in the fact that this would be the first ever mission to collect solid, liquid and gas samples from Titan and also return them to Earth for further analysis.

Acknowledgments

The present mission concept was developed as part of the 2022 edition of Caltech Space Challenge (CSC). This is a one week course organized by Caltech and NASA JPL focused on developing complex mission design concepts starting from a given set of mission objectives and constraints. Team Voyager would like to thank Caltech, NASA JPL, Keck Institute for Space Studies, the organizing team, the sponsors of the competition, and the mentors that helped us throughout the mission formulation effort.

References

[1] Lopes, R. M., Malaska, M., Schoenfeld, A. M., Solomonidou, A., Birch, S., Florence, M., Hayes, A., Williams, D., Radebaugh, J., Verlander, T., et al., "A global geomorphologic map of Saturn's moon Titan," *Nature astronomy*, Vol. 4, No. 3, 2020, pp. 228–233.

[2] Atreya, S. K., Lorenz, R. D., and Waite, J. H., "Volatile origin and cycles: nitrogen and methane," *Titan from Cassini-Huygens*, Springer, 2009, pp. 177–199.

[3] Niemann, H., Atreya, S., Bauer, S., Carignan, G., Demick-Montelara, J., Frost, R., Gautier, D., Haberman, J., Harpold, D., Hunten, D., et al., "Results from the Gas Chromatograph Mass Spectrometer (GCMS) Experiment on the Cassini-Huygens Probe," *AGU Fall Meeting Abstracts*, Vol. 2005, 2005, pp. P43B–03.

[4] Tyler, G., Eshleman, V., Anderson, J., Levy, G., Lindal, G., Wood, G., and Croft, T., "Radio science investigations of the Saturn system with Voyager 1: Preliminary results," *Science*, Vol. 212, No. 4491, 1981, pp. 201–206.

[5] Stofan, E. R., Elachi, C., Lunine, J. I., Lorenz, R. D., Stiles, B., Mitchell, K., Ostro, S., Soderblom, L., Wood, C., Zebker, H., et al., "The lakes of Titan," *Nature*, Vol. 445, No. 7123, 2007, pp. 61–64.

[6] Jennings, D., Tokano, T., Cottini, V., Nixon, C., Achterberg, R., Flasar, F., Kunde, V., Romani, P., Samuelson, R., Segura, M., et al., "Titan surface temperatures during the Cassini mission," *The Astrophysical Journal Letters*, Vol. 877, No. 1, 2019, p. L8.

[7] Hayes, A. G., Lorenz, R. D., and Lunine, J. I., "A post-Cassini view of Titan's methane-based hydrologic cycle," *Nature Geoscience*, Vol. 11, No. 5, 2018, pp. 306–313.

[8] Lunine, J. I., and Atreya, S. K., "The methane cycle on Titan," *Nature Geoscience*, Vol. 1, No. 3, 2008, pp. 159–164.

[9] Hörst, S. M., "Titan's atmosphere and climate," *Journal of Geophysical Research: Planets*, Vol. 122, No. 3, 2017, pp. 432–482.

[10] Glein, C. R., and Shock, E. L., "A geochemical model of non-ideal solutions in the methane–ethane–propane–nitrogen–acetylene system on Titan," *Geochimica et Cosmochimica Acta*, Vol. 115, 2013, pp. 217–240.

[11] Tan, S. P., Kargel, J. S., Jennings, D. E., Mastrogiuseppe, M., Adidharma, H., and Marion, G. M., "Titan's liquids: Exotic behavior and its implications on global fluid circulation," *Icarus*, Vol. 250, 2015, pp. 64–75.

[12] Tan, S. P., and Kargel, J. S., "Multiphase-equilibria analysis: Application in modeling the atmospheric and lacustrine chemical systems of Saturn's moon Titan," *Fluid Phase Equilibria*, Vol. 458, 2018, pp. 153–169.

[13] Hayes, A. G., "The lakes and seas of Titan," *Annual Review of Earth and Planetary Sciences*, Vol. 44, 2016, pp. 57–83.

[14] Lorenz, R. D., "The challenging depths of Titan's seas," *Journal of Geophysical Research: Planets*, Vol. 126, No. 4, 2021, p. e2020JE006786.

[15] McKay, C., and Smith, H., "Possibilities for methanogenic life in liquid methane on the surface of Titan," *Icarus*, Vol. 178, No. 1, 2005, pp. 274–276.

[16] Schulze-Makuch, Dirk, Grinspoon, and H, D., "Biologically enhanced energy and carbon cycling on Titan?" *Astrobiology*, Vol. 5, No. 4, 2005, pp. 560–567.

[17] Barnes, J. W., Turtle, E. P., Trainer, M. G., Lorenz, R. D., MacKenzie, S. M., Brinckerhoff, W. B., Cable, M. L., Ernst, C. M., Freissinet, C., Hand, K. P., et al., "Science goals and objectives for the Dragonfly Titan rotorcraft relocatable lander," *The Planetary Science Journal*, Vol. 2, No. 4, 2021, p. 130.

[18] Lorenz, R. D., Turtle, E. P., Barnes, J. W., Trainer, M. G., Adams, D. S., Hibbard, K. E., Sheldon, C. Z., Zacny, K., Peplowski, P. N., Lawrence, D. J., et al., "Dragonfly: A rotorcraft lander concept for scientific exploration at Titan," *Johns Hopkins APL Technical Digest*, Vol. 34, No. 3, 2018, p. 14.

[19] of Sciences Engineering, N. A., and Medicine", "Origins, Worlds, and Life: A Decadal Strategy for Planetary Science and Astrobiology 2023-2032," 2022.

[20] Russell, C. T., *The Cassini-Huygens Mission*, KLUWER, 2002.

[21] Raulin, F., Coll, P., Coscia, D., Gazeau, M., Sternberg, R., Bruston, P., Israel, G., and Gautier, D., "An exobiological view of Titan and the Cassini-Huygens mission," *Advances in Space Research*, Vol. 22, No. 3, 1998, pp. 353–362.

[22] Raulin, F., Brassé, C., Poch, O., and Coll, P., "Prebiotic-like chemistry on Titan," *Chemical Society Reviews*, Vol. 41, No. 16, 2012, pp. 5380–5393.

[23] Mahaffy, P. R., Webster, C. R., Cabane, M., Conrad, P. G., Coll, P., Atreya, S. K., Arvey, R., Barciniak, M., Benna, M., Bleacher, L., et al., "The sample analysis at Mars investigation and instrument suite," *Space Science Reviews*, Vol. 170, No. 1, 2012, pp. 401–478.

[24] Brinckerhoff, W. B., Pinnick, V. T., Van Amerom, F. H., Danell, R. M., Arevalo, R. D., Atanassova, M. S., Li, X., Mahaffy, P. R., Cotter, R. J., Goesmann, F., et al., "Mars Organic Molecule Analyzer (MOMA) mass spectrometer for ExoMars 2018 and beyond," *2013 IEEE Aerospace Conference*, IEEE, 2013, pp. 1–8.

[25] Wiens, R. C., Maurice, S., and Rull Perez, F., "The SuperCam remote sensing instrument suite for the Mars 2020 rover mission: A preview," *Spectroscopy*, Vol. 32, No. LA-UR-17-26876, 2017.

[26] Wiens, R. C., Maurice, S., Robinson, S. H., Nelson, A. E., Cais, P., Bernardi, P., Newell, R. T., Clegg, S., Sharma, S. K., Storms, S., et al., "The SuperCam instrument suite on the NASA Mars 2020 rover: Body unit and combined system tests," *Space Science Reviews*, Vol. 217, No. 1, 2021, pp. 1–87.

[27] Xu, W., Liu, X., Yan, Z., Li, L., Zhang, Z., Kuang, Y., Jiang, H., Yu, H., Yang, F., Liu, C., et al., "The MarSCoDe instrument suite on the Mars Rover of China's Tianwen-1 mission," *Space Science Reviews*, Vol. 217, No. 5, 2021, pp. 1–58.

[28] Sobron, P., Barge, L. M., Amend, J., Burnett, J., Detry, R., Doloboff, I., Kelley, D. S., Marburg, A., Misra, A. K., Nawaz, A., et al., "Exploring underwater vent systems: New technologies and strategies to advance life detection and scientific understanding of ocean worlds," *AGU Fall Meeting Abstracts*, Vol. 2018, 2018, pp. P33G–3903.

[29] Sobron, P., Barge, L., and Team, I., "Exploring Deep Sea Hydrothermal Vents on Earth and Ocean Worlds," *Lunar and Planetary Science Conference*, 2021, p. 2505.

[30] Wiens, R. C., Maurice, S., Barraclough, B., Saccoccio, M., Barkley, W. C., Bell, J. F., Bender, S., Bernardin, J., Blaney, D., Blank, J., et al., "The ChemCam instrument suite on the Mars Science Laboratory (MSL) rover: Body unit and combined system tests," *Space science reviews*, Vol. 170, No. 1, 2012, pp. 167–227.

[31] Veneranda, M., Lopez-Reyes, G., Manrique-Martinez, J. A., Sanz-Arranz, A., Lalla, E., Konstantinidis, M., Moral, A., Medina, J., and Rull, F., "ExoMars Raman Laser Spectrometer (RLS): Development of chemometric tools to classify ultramafic igneous rocks on Mars," *Scientific Reports*, Vol. 10, No. 1, 2020, pp. 1–14.

[32] Uckert, K., Bhartia, R., Beegle, L. W., Monacelli, B., Asher, S. A., Burton, A. S., Bykov, S. V., Davis, K., Fries, M. D., Jakubek, R. S., et al., "Calibration of the SHERLOC Deep Ultraviolet Fluorescence–Raman Spectrometer on the Perseverance Rover," *Applied Spectroscopy*, Vol. 75, No. 7, 2021, pp. 763–773.

[33] Bell, J., Maki, J., Mehall, G., Ravine, M., Caplinger, M., and Team, M.-Z., "MastCam-Z: designing a geologic, stereoscopic, and multispectral pair of zoom cameras for the NASA Mars 2020 rover," *3rd International Workshop on Instrumentation for Planetary Mission*, Vol. 1980, 2016, p. 4126.

[34] Bell, J., Maki, J., Mehall, G., Ravine, M., Caplinger, M., Bailey, Z., Brylow, S., Schaffner, J., Kinch, K., Madsen, M., et al., "The Mars 2020 perseverance rover mast camera zoom (Mastcam-Z) multispectral, stereoscopic imaging investigation," *Space science reviews*, Vol. 217, No. 1, 2021, pp. 1–40.

[35] Kinch, K., Madsen, M., Bell, J., Maki, J., Bailey, Z., Hayes, A., Jensen, O., Merusi, M., Bernt, M., Sørensen, A., et al., "Radiometric calibration targets for the Mastcam-Z Camera on the Mars 2020 Rover mission," *Space science reviews*, Vol. 216, No. 8, 2020, pp. 1–51.

[36] Strange, N., Spilker, T., Landau, D., Lam, T., Lyons, D., and Guzman, J., "Mission design for the titan saturn system mission concept," *Advances in the Astronautical Sciences*, Vol. 135, No. 2, 2009, pp. 919–934.

[37] Matson, D. L., Spilker, L. J., and Lebreton, J.-P., "The Cassini/Huygens mission to the Saturnian system," *The Cassini-Huygens Mission*, Springer, 2003, pp. 1–58.

[38] Muirhead, B. K., Nicholas, A. K., Umland, J., Sutherland, O., and Vijendran, S., "Mars sample return campaign concept status," *Acta Astronautica*, Vol. 176, 2020, pp. 131–138.

[39] Boca, A., Warwick, R., White, B., and Ewell, R., "A data-driven evaluation of the viability of solar arrays at Saturn," *IEEE Journal of Photovoltaics*, Vol. 7, No. 4, 2017, pp. 1159–1164.

[40] Yaghoubi, D., and Ma, P., "Integrated Design Results for the MSR DAC-0.0 Mars Ascent Vehicle," *2021 IEEE Aerospace Conference (50100)*, 2021, pp. 1–17. https://doi.org/10.1109/AERO50100.2021.9438481.

[41] Landis, G. A., Oleson, S. R., Turnbull, E. R., Lorenz, R. D., Smith, D. A., Packard, T., Gyekenyesi, J. Z., Colozza, A. J., and Fittje, J. E., "Mission Incredible: A Titan Sample Return Using In-Situ Propellants," *AIAA SciTech 2022 Forum*, 2022. https://doi.org/10.2514/6.2022-1570.

[42] Donahue, B., "Titan Sample Return Mission Concept," 2010.

[43] Strange, N., Landau, D., Hofer, R., Snyder, J., Randolph, T., Campagnola, S., Szabo, J., and Pote, B., *Solar Electric Propulsion Gravity-Assist Tours For Jupiter Missions*, ???? https://doi.org/10.2514/6.2012-4518, URL https://arc.aiaa.org/doi/abs/10.2514/6.2012-4518.

[44] Jim taylor, L. S., and Wong, C.-J., "Cassini Orbiter/ Huygens Probe Telecommunications," , 2002. URL https://descanso.jpl.nasa.gov/DPSummary/Descanso3--Cassini2.pdf.

[45] Jim Taylor, D. L., and Shambayati, S., "Mars Reconnaissance Orbiter Telecommunications," , 2006. URL https://descanso.jpl.nasa.gov/DPSummary/MRO_092106.pdf.

[46] Mukai, R., Hansen, D., Mittskus, A., Taylor, J., and Danos, M., "Juno Telecommunications," , 2012. URL https://descanso.jpl.nasa.gov/DPSummary/Juno_DESCANSO_Post121106H--Compact.pdf.

[47] Levine, J., and Wright, H., "Cassini Orbiter/ Huygens Probe Telecommunications," , 2005. URL https://ntrs.nasa.gov/api/citations/20050212185/downloads/20050212185.pdf.

[48] Jim Taylor, "The Deep Space Network: A Functional Description," , 2016. URL https://descanso.jpl.nasa.gov/monograph/series13/DeepCommo_Chapter2--141029.pdf, [Online; accessed 25-March-2022].

[49] Systems, K. M., "UUV-3500 SIDE SCAN / BATHYMETRY SONAR SYSTEM HIGH-RESOLUTION SIDE SCAN SONAR FOR UNMANNED UNDERWATER VEHICLES (UUV'S)," http://www.kleinmarinesystems.com/PDF/datasheets/Klein_UUV_3500_rev0718.pdf, ????

[50] Miguel-Soto, D., Leandro, D., Lopez-Aldaba, A., Beato-López, J. J., Pérez-Landazábal, J. I., Auguste, J.-L., Jamier, R., Roy, P., Lopez-Amo, M., et al., "Study of optical fiber sensors for cryogenic temperature measurements," *Sensors*, Vol. 17, No. 12, 2017, p. 2773.

[51] Institute, N. D., "MATERIALS FOR CRYOGENIC SERVICE: ENGINEERING PROPERTIES OF AUSTENITIC STAINLESS STEELS," 1974.

[52] Bosanac, N., Marsden, J. E., Moore, A., and Campagnola, S., "TITAN TRAJECTORY DESIGN USING INVARIANT

MANIFOLDS AND RESONANT GRAVITY ASSISTS," ????, p. 14.
[53] Gawlik, E. S., Marsden, J. E., Campagnola, S., and Moore, A., "Invariant Manifolds, Discrete Mechanics, and Trajectory Design for a Mission to Titan," *19th AAS/AIAA Space Flight Mechanics Meeting*, Savannah, Georgia, 2009.
[54] Vaquero, M., and Howell, K. C., "Transfer Design Exploiting Resonant Orbits and Manifolds in the Saturn–Titan System," *Journal of Spacecraft and Rockets*, Vol. 50, No. 5, 2013, pp. 1069–1085. https://doi.org/10.2514/1.A32412.
[55] Sims, J., and Longuski, J., *Analysis of V(infinity) leveraging for interplanetary missions*, ???? https://doi.org/10.2514/6.1994-3769, URL https://arc.aiaa.org/doi/abs/10.2514/6.1994-3769.
[56] Rodríguez, J. L. C., Eichhorn, H., and McLean, F., "POLIASTRO: AN ASTRODYNAMICS LIBRARY WRITTEN IN PYTHON WITH FORTRAN PERFORMANCE," ????, p. 8.
[57] Wertz, J. R., Everett, D. F., and Puschell, J. J., *Space Mission Engineering: The New SMAD*, 7th ed., Microcosm Press, 2011.
[58] Release, N. P., "NASA Selects Developer for Rocket to Retrieve First Samples from Mars," , February 2022. URL https://www.nasa.gov/press-release/nasa-selects-developer-for-rocket-to-retrieve-first-samples-from-mars.
[59] Tate, R., "Light weight radioisotope heater unit (LWRHU): a technical description of the reference design," Tech. rep., Los Alamos National Lab., NM (USA), 1982.
[60] Kantsiper, B., "The Double Asteroid Redirection Test (DART) mission electric propulsion trade," *2017 IEEE Aerospace Conference*, 2017, pp. 1–7. https://doi.org/10.1109/AERO.2017.7943736.
[61] Low, S. Y. W., and Chia, Y. X., "Assessment of Orbit Maintenance Strategies for Small Satellites," *AIAA / USU Small Satellite Conference*, 2018.
[62] Durante, D., Hemingway, D., Racioppa, P., Iess, L., and Stevenson, D., "Titan's gravity field and interior structure after Cassini," *Icarus*, Vol. 326, 2019, pp. 123–132. https://doi.org/https://doi.org/10.1016/j.icarus.2019.03.003, URL https://www.sciencedirect.com/science/article/pii/S0019103518307267.
[63] Cruz, J. R., Cianciolo, A. D., Powell, R. W., Simonsen, L. C., and Tolson, R. H., "Entry, Descent, and Landing Technology Concept Trade Study for Increasing Payload Mass to the Surface of Mars," *4th International Symposium on Atmospheric Reentry Vehicles and Systems*, 2005. https://doi.org/https://doi.org/10.1029/2005JE002649, URL https://ntrs.nasa.gov/citations/20050158774.
[64] Roelke, E., and Braun, R., "Trajectory Trade-space Design for Robotic Entry at Titan," Ph.D. thesis, Georgia Institute of Technology, 2017.
[65] Dec, J. A., and Braun, R. D. (eds.), *An Approximate Ablative Thermal Protection System Sizing Tool for Entry System Design*, AIAA, 2006.
[66] NASA, "Phenolic-Impregnated Carbon Ablator (PICA) Heat Shield Technology is Used by SpaceX," , 2015. URL https://www.nasa.gov/offices/oct/images/phenolic-impregnated-carbon-ablator-pica-heat-shield-technology-is-used-by-spacex, [Online; accessed 26-March-2022].
[67] Yang, W., Liu, J., Wang, Y., and Gao, S., "Experimental study on the thermal conductivity of aerogel-enhanced insulating materials under various hygrothermal environments," *Energy and Buildings*, Vol. 206, 2020, p. 109583.
[68] Plastics, L., "Technical Data Sheet: G-10," , ???? URL https://laminatedplastics.com/g-10.pdf.
[69] Company, S. S., "Specification Sheet: Alloy 316/316L," , ???? URL https://www.sandmeyersteel.com/images/316-316l-317l-spec-sheet.pdf.
[70] Yaghoubi, D., and Schnell, A., "Mars Ascent Vehicle Solid Propulsion Configuration," *2020 IEEE Aerospace Conference*, 2020, pp. 1–11. https://doi.org/10.1109/AERO47225.2020.9172654.
[71] Amanda R Hendrix1, Y. L. Y., "Energy Options for Future Humans on Titan," *Astrobiology & Outreach*, Vol. 5, No. 2, 2017, pp. 2–4.
[72] et. al, G. D., "The Global Precipitation Measurement (GPM) Spacecraft Power System Design and Orbital Performance," *ESP Sciences*, 2016, pp. 3–4.
[73] "ABSL Performance Comparison," , 2011. URL https://www.nasa.gov/sites/default/files/atoms/files/01_absl_2011_nasa_battery_workshop.pdf.
[74] "LMolicel Data Sheet," , ???? URL https://www.molicel.com/wp-content/uploads/DM_ICR18650M-V3-80072.pdf.
[75] Sonneveldt, B., Kim, H., Pruitt, M., Hissam, D. A., and Cormarkovic, V., "Mars Ascent Vehicle (MAV) concept - launch system development," , 2017. https://doi.org/2014/46266, URL https://hdl.handle.net/2014/46266.
[76] Hurlbert, E. A., Ueno, H., Alexander, L., Klem, M. D., Daversa, E., Rualt, J.-M., Manfletti, C., Caruana, J.-N., Asakawa, H., and Whitley, R. J., *International Space Exploration Coordination Group Assessment of Technology Gaps for LOx/Methane Propulsion Systems for the Global Exploration Roadmap*, ???? https://doi.org/10.2514/6.2016-5280, URL https://arc.aiaa.org/doi/abs/10.2514/6.2016-5280.
[77] Fulchignoni, M., Ferri, F., and Angrilli, F., "In situ measurements of the physical characteristics of Titan's environment," *Nature*, 2006. https://doi.org/10.1038/nature04314.
[78] Boone, D. R., "Titan Atmospheric Density Results from Cassini's T107 Flyby," *Proceedings of the 25th International Symposium on Space Flight Dynamics*, 2015.
[79] Sutton, G. P., and Biblarz, O., *Rocket Propulsion Elements*, 9th ed., Wiley, 2016.
[80] Cantera Developers, "Cantera," , ???? URL https://cantera.org/install/index.html.
[81] Sanchez, H., McIntosh, D., Cannon, H., Pires, C., Sullivan, J., D'Amico, S., and O'Connor, B., "Starling1: Swarm Technology Demonstration," *AIAA / USU Small Satellite Conference*, 2018.

[82] Mortari, D., Junkins, J. L., and Samaan, M., "Lost-in-space pyramid algorithm for robust star pattern recognition," *Guidance and control 2001*, 2001, pp. 49–68.

[83] D'Amico, S., "Autonomous Formation Flying in Low Earth Orbit," Ph.D. thesis, TU Delft, 2010.

[84] Kruger, J., and D'Amico, S., "Autonomous angles-only multitarget tracking for spacecraft swarms," *Acta Astronautica*, Vol. 189, 2021, pp. 514–529. https://doi.org/https://doi.org/10.1016/j.actaastro.2021.08.049, URL https://www.sciencedirect.com/science/article/pii/S0094576521004707.

[85] Yasuda Seiji, K. T., Matsushima Kota, "Hayabusa2 — Autonomous Navigation, Guidance and Control System Supported Pinpoint Touchdowns on Asteroid Ryugu," *NEC Technical Journal*, Vol. 16, 2021, pp. 123–132. URL https://www.nec.com/en/global/techrep/journal/g21/n01/pdf/210128.pdf?fromPDF_E7401.

[86] NASA, "Cassini Orbiter/Huygens Probe Telecommunications," , 2002. URL https://descanso.jpl.nasa.gov/DPSummary/Descanso3--Cassini2.pdf, [Online; accessed 25-March-2022].

[87] NASA, "Titan Explorer: - NASA Technical Reports Server," , 2005. URL https://ntrs.nasa.gov/api/citations/20050212185/downloads/20050212185.pdf, [Online; accessed 25-March-2022].

[88] JPL, "Small Deep Space Transponder (SDST) DS1 Technology Validation Report," , 2005. URL https://pdssbn.astro.umd.edu/holdings/ds1-c-micas-3-rdr-visccd-borrelly-v1.0/document/doc_Apr04/int_reports/SDST_Integrated_Report.pdf, [Online; accessed 25-March-2022].

[89] NASA, "Mars Reconnaissance Orbiter Telecommunications," , 2006. URL https://descanso.jpl.nasa.gov/DPSummary/MRO_092106.pdf, [Online; accessed 25-March-2022].

[90] Weekley, J. M., and Mangus, B. J., "TWTA versus SSPA: A comparison of on-orbit reliability data," *IEEE Transactions on Electron Devices*, Vol. 52, No. 5, 2005, pp. 650–652.

[91] NASA, "Ka Band 100W Solid State Power Amplifier (SSPA)," , 2017. URL https://www.esa.int/Enabling_Support/Space_Engineering_Technology/Shaping_the_Future/Ka_Band_100W_Solid_State_Power_Amplifier_SSPA, [Online; accessed 25-March-2022].

[92] JPL, "The MarCO Mission from a Telecom Perspective, Highlighting the First Use of the Iris Deep Space Transponder," , 2017. URL https://www.esa.int/Enabling_Support/Space_Engineering_Technology/Shaping_the_Future/Ka_Band_100W_Solid_State_Power_Amplifier_SSPA, [Online; accessed 25-March-2022].

[93] Luo, X., Ouyang, J., Chen, Z.-H., Yan, Y., Han, L., Wu, Z., Yu, T., and Zheng, K., "A scalable Ka-band 1024-element transmit dual-circularly-polarized planar phased array for SATCOM application," *IEEE Access*, Vol. 8, 2020, pp. 156084–156095.